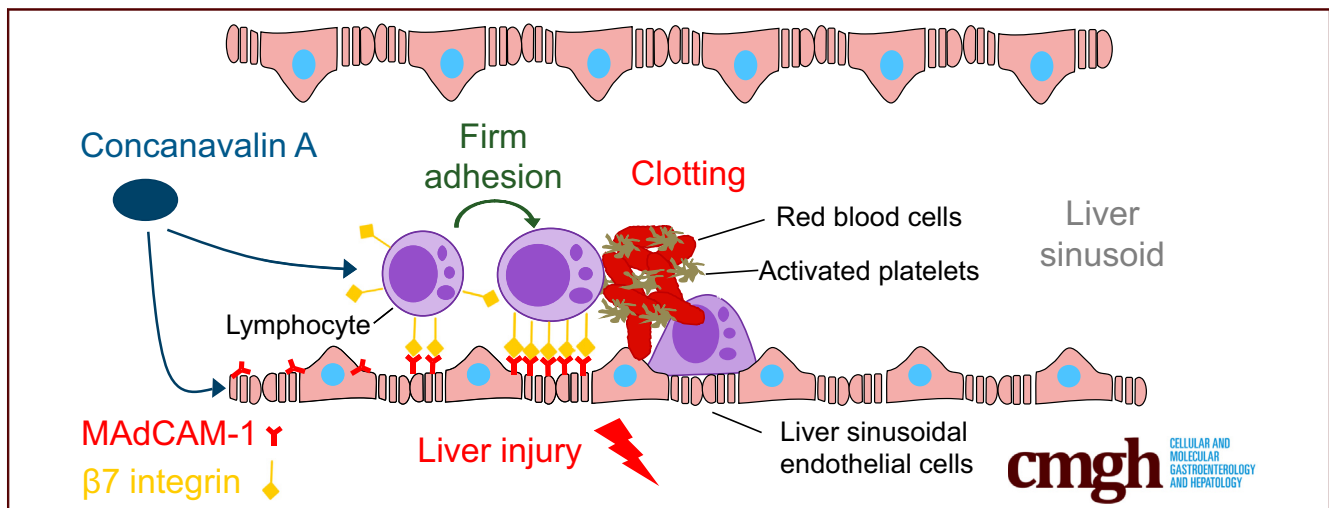


ORIGINAL RESEARCH

MAdCAM-1/ $\alpha 4\beta 7$ Integrin-Mediated Lymphocyte/Endothelium Interactions Exacerbate Acute Immune-Mediated Hepatitis in Mice

Angela Schippers,^{1,*} Jessica Hübel,^{1,*} Felix Heymann,^{2,*} Thomas Clahsen,¹ Sreepadha Eswaran,¹ Sarah Schlepütz,¹ Robin Püllen,¹ Nikolaus Gaßler,³ Klaus Tenbrock,¹ Frank Tacke,² and Norbert Wagner¹

¹Department of Pediatrics, Medical Faculty, RWTH Aachen University, Aachen, Germany; ²Department of Hepatology and Gastroenterology, Charité University Medicine Berlin, Berlin, Germany; and ³Institute of Forensic Medicine, Section of Pathology, Jena University Hospital, Jena, Germany



SUMMARY

Mucosal addressin cell-adhesion molecule-1 (MAdCAM-1)-deficient mice show decreased susceptibility to concanavalin A (ConA)-induced hepatitis. ConA causes reduced motility and increased adhesion of lymphocytes in liver sinusoids, which depends on MAdCAM-1. $\beta 7$ integrin expression contributes to MAdCAM-1 upregulation and liver damage.

BACKGROUND & AIMS: Aberrant lymphocyte homing could potentially link inflammatory processes in the intestine and the liver, as distinct hepatobiliary diseases frequently develop as extra-intestinal manifestations in inflammatory bowel disease. In this study, we examined the role of the gut-tropic leukocyte adhesion molecule $\beta 7$ integrin and its endothelial ligand mucosal addressin cell-adhesion molecule-1 (MAdCAM-1) in immune-mediated hepatitis in mice.

METHODS: Wild-type (WT) mice, MAdCAM-1-deficient mice, $\beta 7$ integrin-deficient mice, RAG-2-deficient mice, RAG-2/MAdCAM-1 double-deficient mice, and RAG-2/ $\beta 7$ integrin double-deficient mice were subjected to concanavalin A

(ConA)-induced hepatitis. The degree of hepatitis was evaluated by histology, flow cytometry, and expression analysis of inflammatory mediators. The motility of lymphocytes in progressive liver damage was assessed by intravital laser scanning multiphoton microscopy.

RESULTS: Ablation of MAdCAM-1 or $\beta 7$ integrin ameliorated ConA-induced hepatitis in mice. $\beta 7$ integrin-deficient lymphocytes caused less liver damage than WT lymphocytes in ConA-treated RAG-2-deficient mice. Moreover, WT lymphocytes caused less liver damage in ConA-treated RAG-2/ $\beta 7$ integrin double-deficient mice than in similarly treated RAG-2-deficient mice, indicating that $\beta 7$ integrin expression contributes significantly to the liver damage mediated by innate immune cells. MAdCAM-1 expression was dependent on $\beta 7$ integrin expression on adaptive and innate immune cells. Most importantly, lymphocytes in ConA-treated MAdCAM-1-deficient mice displayed more motility and less adhesion in the liver sinusoids *in vivo*, than lymphocytes in similarly treated WT mice.

CONCLUSIONS: These data suggest that $\beta 7$ integrin expression on lymphocytes and innate immune cells contributes to MAdCAM-1 upregulation and liver damage in acute immune-mediated hepatitis, most likely by facilitating lymphocyte/sinusoidal endothelial cell interactions. (*Cell Mol*

Gastroenterol Hepatol 2021;11:1227–1250; <https://doi.org/10.1016/j.jcmgh.2020.12.003>

Keywords: Adhesion Molecules; Concanavalin A; Cell Migration.

The concanavalin A (ConA) model is an established mouse model for the study of pathogenic mechanisms of acute immune-mediated liver injury, with features resembling viral and autoimmune hepatitis.¹ Intravenous injection of ConA induces massive hepatocyte necrosis and marked infiltration of lymphocytes into the liver and is accompanied by dramatic changes in the intrahepatic expression of proinflammatory genes such as *Tnf- α* , *Ifn- γ* , *Il-2*, *Il-4*, and *Il-6*.^{2–4} In addition to CD4⁺ T cells, CD8⁺ T cells, natural killer T (NKT) cells, neutrophils, and Kupffer cells (KCs) contribute to the inflammatory process.^{1,4}

Lymphocyte adhesion and transmigration through the endothelial cell barrier into tissue is an important feature of the response of effector cells to inflammatory conditions, a multistep process regulated by chemokines and adhesion molecules.⁵ Owing to the crucial role of adhesion molecules in inflammation, a number of studies have been conducted to evaluate their role in ConA-induced hepatitis. L-selectin, or ICAM-1 (intercellular adhesion molecule-1) were shown to contribute cooperatively to ConA-induced hepatitis by regulating the influx of CD4⁺ cells.⁶ Likewise, P-selectin was found to promote liver injury.⁷ E-selectin and vascular cell adhesion molecule-1 (VCAM-1) are strongly expressed in inflammatory liver diseases.^{8,9} Immunoneutralization of E-selectin or VCAM-1 improves intrahepatic blood flow and reduces hepatic injury in the ConA model.¹⁰ Moreover, LFA-1 (lymphocyte function-associated antigen-1) expression on T cells was shown to promote ConA-induced liver damage,¹¹ while $\alpha 4\beta 1$ integrin was found to mediate adhesion of CD4⁺ T helper (Th1) cells to sinusoidal liver vessels.¹² However, the contributions of $\beta 7$ integrin and mucosal addressin cell adhesion molecule-1 (MAdCAM-1) to the pathogenesis of ConA-mediated hepatitis have not yet been investigated.

The lymphocyte adhesion molecule $\beta 7$ integrin forms heterodimers with either the $\alpha 4$ or the αE (CD103) subunit. $\alpha 4\beta 7$ integrin is expressed on activated gut-homing CD4⁺ T-cells, NK cells, activated monocytes, macrophages, eosinophils, and dendritic cells (DCs).¹³ It directs the migration of lymphocytes into the small intestine and into the mesenteric lymph nodes, mainly via interaction with its endothelial ligand MAdCAM-1.^{13,14} MAdCAM-1 is predominantly expressed on high endothelial venules of gut-associated lymphoid tissue and on venules at chronically inflamed sites.¹³ It is widely accepted that $\alpha 4\beta 7$ /MAdCAM-1 interactions play a role in promoting intestinal inflammation.¹³ Patients suffering from inflammatory bowel disease (IBD) have a tendency to develop extraintestinal disorders such as primary sclerosing cholangitis.¹⁵ Although MAdCAM-1 is only expressed in minute amounts in healthy liver,¹⁶ it is upregulated in association with portal tract inflammation,¹⁷ where it is able to support the adhesion of $\alpha 4\beta 7$ ⁺ gut-derived lymphocytes.¹⁸ Moreover, it is upregulated in the cirrhotic liver.¹⁶ These findings gave rise to the

hypothesis that common mechanisms control lymphocyte homing to the inflamed liver and gut.¹⁹ A thorough analysis of immune cell migration pathways that could be targeted therapeutically in different liver diseases would therefore seem worthwhile.

Recently, we have shown that MAdCAM-1 deficiency ameliorates experimental nonalcoholic steatohepatitis while $\beta 7$ integrin deficiency worsens the outcome in mice.²⁰ Utilizing the ConA model, we compared wild-type (WT) with adhesion molecule-deficient mice ($\beta 7$ integrin-deficient mice, MAdCAM-1-deficient mice) and RAG-2 (recombination activating gene-2)-deficient with RAG-2/adhesion molecule double-deficient mice (RAG-2/ $\beta 7$ integrin double-deficient mice, RAG-2/MAdCAM-1 double-deficient mice) after reconstitution with different immune cells, and were thereby able to highlight the critical role of MAdCAM-1 and $\alpha 4\beta 7$ integrin in the pathogenesis of acute immune-mediated hepatitis.

Results

MAdCAM-1- and $\beta 7$ Integrin-Deficient Mice Are Protected From ConA-Mediated Liver Injury

To determine the role of $\alpha 4\beta 7$ integrin/MAdCAM-1 interactions in the development of acute hepatitis, $\beta 7$ integrin-deficient ($\beta 7 \Delta/\Delta$), MAdCAM-1-deficient (MAdCAM-1 Δ/Δ), and WT mice were subjected to intravenous ConA injection. Eight hours following ConA administration, the plasma levels of both alanine aminotransferase and aspartate aminotransferase were found to be markedly increased in WT mice. In contrast, $\beta 7$ integrin-deficient mice exhibited a 5-fold reduction in aminotransferase levels, while in MAdCAM-1-deficient mice, an up to 10-fold reduction was observed (Figure 1A and data not shown). After 20 hours of ConA challenge, liver aminotransferase levels were still markedly reduced in mutant mice compared with WT mice, although the attenuation effect was less pronounced in the $\beta 7$ integrin-deficient mice (Figure 1A). Without treatment, hematoxylin and eosin (H&E)-stained liver sections from WT and mutant mice appeared histologically identical. After 8 hours of ConA administration, only slight degenerative changes and necrosis were observed and although mutant mice exhibited a trend toward decreased necrosis, compared with WT mice, no significant difference was found. In contrast, large bridging necrotic areas were clearly distinguishable from

*Authors share co-first authorship.

Abbreviations used in this paper: BSA, bovine serum albumin; ConA, concanavalin A; DC, dendritic cell; H&E, hematoxylin and eosin; IBD, inflammatory bowel disease; KC, Kupffer cells; MAdCAM-1, mucosal addressin cell-adhesion molecule-1; mRNA, messenger RNA; NK, natural killer; PAI, plasminogen activator inhibitor-1; PBS, phosphate-buffered saline; RT-PCR, real-time polymerase chain reaction; TF, tissue factor; TSA, tyramide signal amplification; TUNEL, terminal deoxynucleotidyl transferase dUTP nick end labeling; VCAM-1, vascular cell adhesion molecule-1; WT, wild-type.

 Most current article

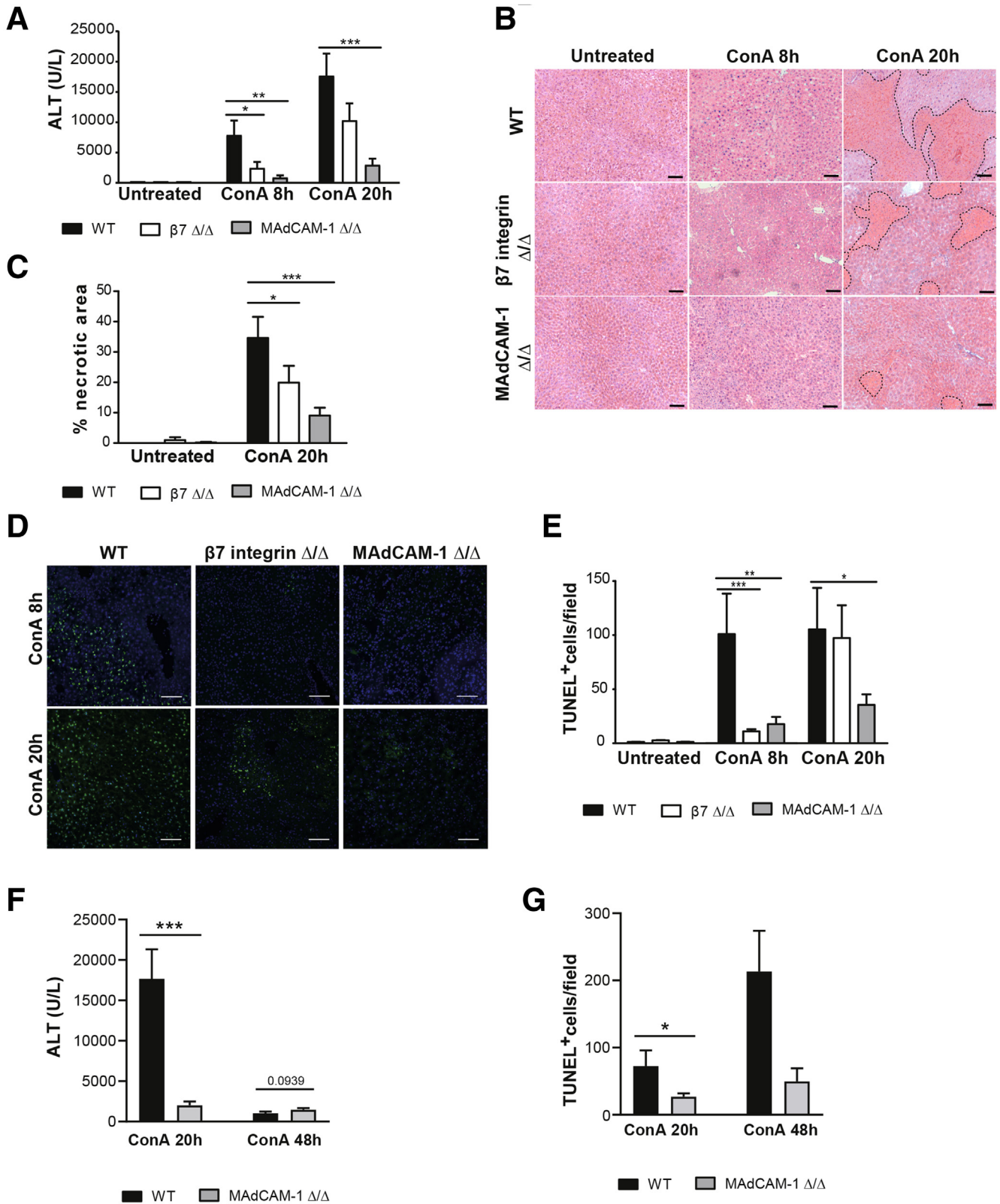
© 2021 The Authors. Published by Elsevier Inc. on behalf of the AGA Institute. This is an open access article under the CC BY-NC-ND license (<http://creativecommons.org/licenses/by-nc-nd/4.0/>).

2352-345X

<https://doi.org/10.1016/j.jcmgh.2020.12.003>

the surrounding hepatic parenchyma in WT livers 20 hours after ConA challenge, whereas the percentage of necrotic lesions in $\beta 7$ integrin-deficient mice was

significantly reduced, and livers of MAdCAM-1-deficient mice had an almost normal histological appearance (Figure 1B and C).



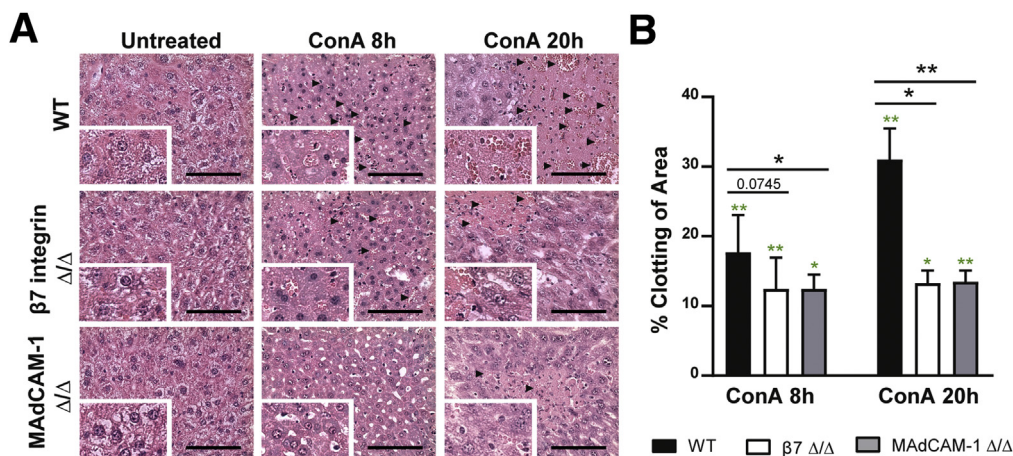


Figure 2. MAdCAM-1- and $\beta 7$ integrin-deficient mice display reduced clotting following ConA treatment. Plasma and liver specimens were sampled at 8 or 20 hours after ConA administration. (A) Representative photomicrographs of H&E-stained liver sections at original magnification $\times 20$. Scale bar = 100 μm . Prominent hemostasis marked by black arrowheads is seen in the sinusoids. (B) Quantification of clotting in H&E-stained liver sections shown as percentage of the section area ($n \geq 6$ mice per group). Data represent mean \pm SEM. Statistical significance was calculated in by the Mann-Whitney nonparametric t test ($*P < .05$, $**P < .01$). WT (black bars), $\beta 7$ integrin Δ/Δ (white bars), and MAdCAM-1 Δ/Δ mice (gray bars).

Staining of liver sections by terminal deoxynucleotidyl transferase dUTP nick end labeling (TUNEL) confirmed extensive hepatocyte apoptosis in WT mice, 8 hours after ConA injection, whereas mutant mice were significantly less affected (Figure 1D and E). Twenty hours after challenge, not only WT, but also $\beta 7$ integrin-deficient mice exhibited massive liver cell apoptosis, whereas apoptosis was almost absent in MAdCAM-1-deficient mice (Figure 1D and E).

To further substantiate that the observed effects caused by MAdCAM-1 deficiency constitute an amelioration and not just a delay in injury formation, we evaluated liver pathogenesis in WT and MAdCAM-1-deficient mice 48 hours after ConA treatment. Also, at this time point we see a succinct difference in liver damage as estimated by TUNEL staining. WT mice still exhibit more liver cell apoptosis than MAdCAM-1-deficient mice. In contrast, alanine aminotransferase levels have already greatly declined and differences between WT and MAdCAM-1-deficient mice are no longer significant (Figure 1F and G), suggesting that acute inflammation in both mouse strains has already entered the resolution stage.

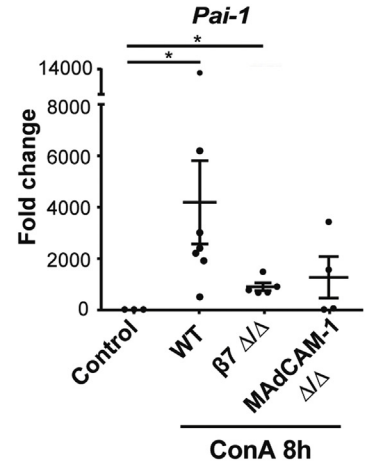
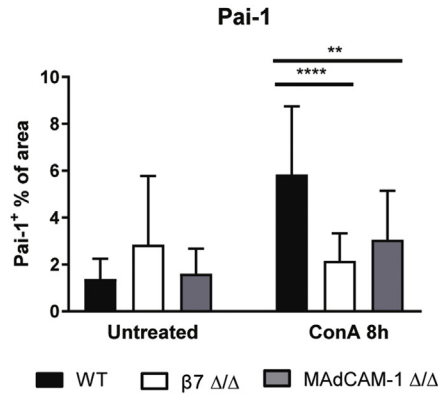
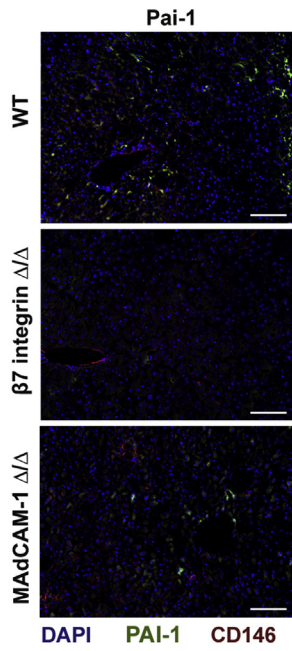
ConA-mediated liver necrosis is reportedly accompanied by thrombocytopenia and intrahepatic hemostasis, which

contribute to liver injury.^{21,22} At 8 and 20 hours after ConA injection, we observed prominent blood clotting in the sinusoids of WT mice, which was significantly less pronounced in $\beta 7$ integrin-deficient and in MAdCAM-1-deficient mice (Figure 2A and B). Tissue factor (TF) and plasminogen activator inhibitor-1 (PAI-1) contribute to ConA-induced hepatic thrombosis.²² Interestingly, decreased coagulation in the livers of ConA-treated MAdCAM-1-deficient or $\beta 7$ integrin-deficient mice was paralleled by a reduction in the expression levels of PAI-1 messenger RNA (mRNA) in liver tissue homogenates (Figure 3A) and a trend toward decreased TF mRNA levels (Figure 3B) 8 hours after ConA administration. These results were confirmed at protein level by immunofluorescence stainings, in which ConA-treated mice lacking MAdCAM-1 or $\beta 7$ integrin showed reduced staining for PAI-1 and TF (Figure 3A and B). These findings were accompanied by a significantly reduced intrahepatic platelet accumulation in mutant mice, as demonstrated by staining for CD41 (Figure 3C).

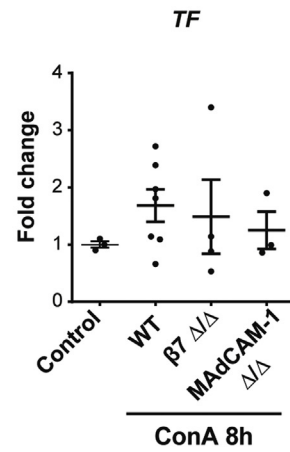
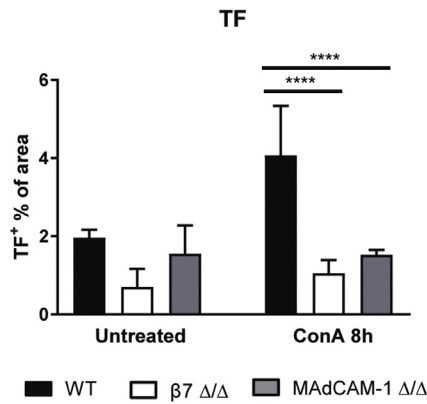
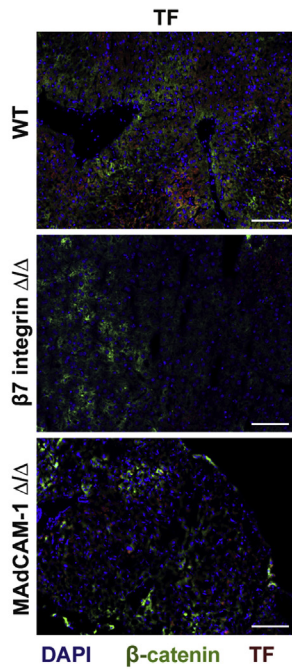
MAdCAM-1 is expressed only minimally in the uninflamed liver.¹⁶ We, therefore, investigated hepatic expression of MAdCAM-1 under inflammatory conditions using

Figure 1. (See previous page). ConA-induced liver damage is ameliorated in MAdCAM-1-deficient and $\beta 7$ integrin-deficient mice. Plasma and liver specimens were sampled at 8, 20, or 48 hours after ConA administration. The data shown are representative of 3 independent experiments. Data represent mean \pm SEM. Statistical significance was calculated in panels A, C, E, F, and G by the Mann-Whitney nonparametric t test ($*P < .05$, $**P < .01$, $***P < .001$). WT (black bars), $\beta 7$ integrin Δ/Δ (white bars), and MAdCAM-1 Δ/Δ mice (gray bars). (A) Quantification of serum alanine aminotransferase (ALT). WT ($n = 9-10$), $\beta 7$ integrin Δ/Δ ($n = 5-11$), and MAdCAM-1 Δ/Δ mice ($n = 7-10$). (B) Representative photomicrographs of H&E-stained liver sections with marked necrotic areas (original magnification $\times 10$; scale bar = 100 μm) and (C) quantification of necrotic area fraction. WT ($n = 4$), $\beta 7$ integrin Δ/Δ ($n = 4-5$), and MAdCAM-1 Δ/Δ mice ($n = 3-4$). (D) Representative photomicrographs (original magnification $\times 10$; scale bar = 100 μm) and (E) quantification of bright green apoptotic cells as detected by TUNEL assay 8 or 20 hours post-ConA injection. WT ($n = 9-12$), $\beta 7$ integrin Δ/Δ ($n = 7-10$), and MAdCAM-1 Δ/Δ mice ($n = 10$), and untreated control mice ($n = 9$ each). (F) Quantification of serum ALT. (WT: $n = 7-9$, MAdCAM-1 Δ/Δ : $n = 9-10$). (G) Quantification of apoptotic cells as detected by TUNEL assay on liver sections. WT: $n = 3-7$, MAdCAM-1 Δ/Δ : $n = 4-10$.

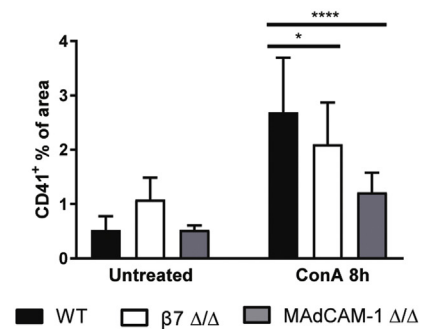
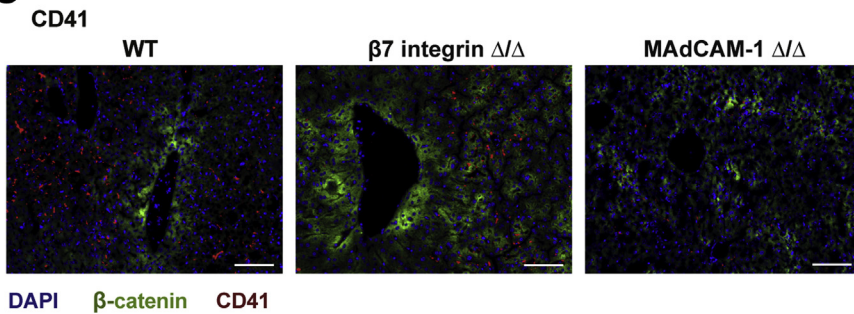
A



B



C



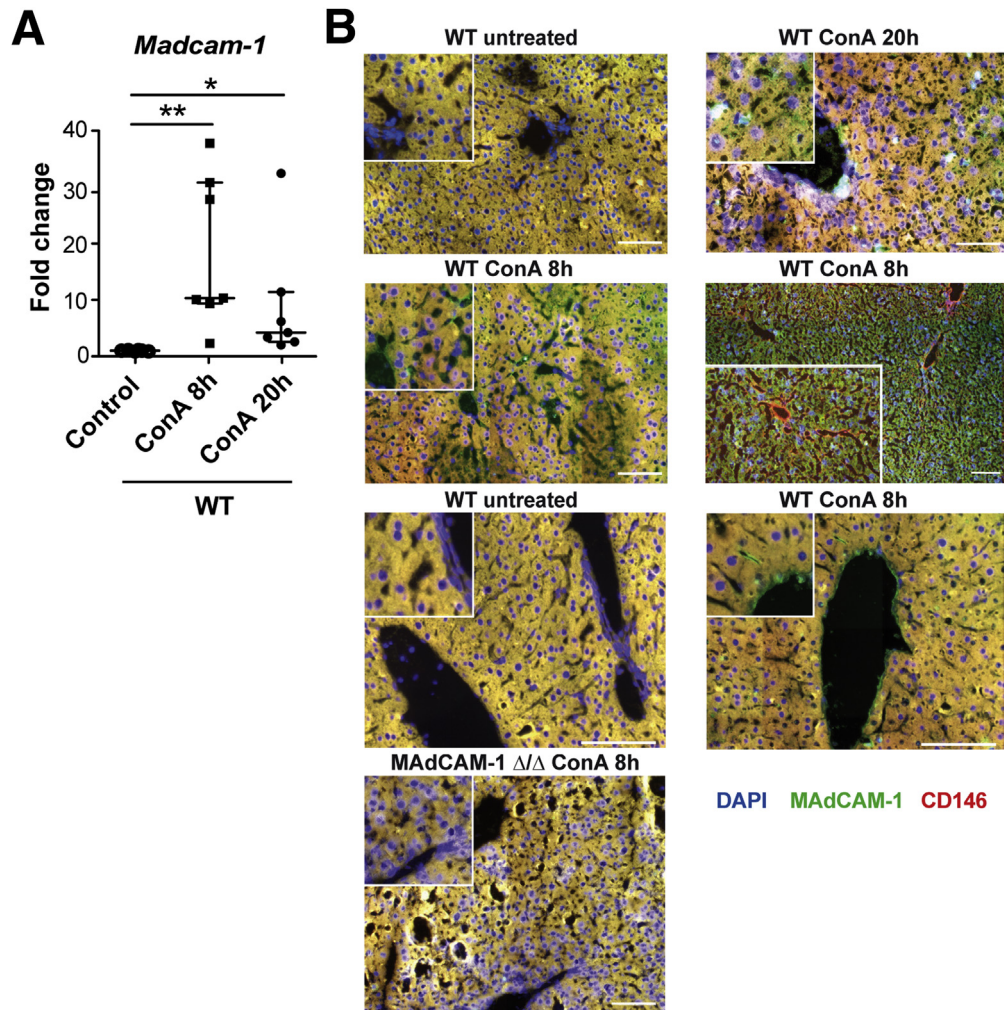
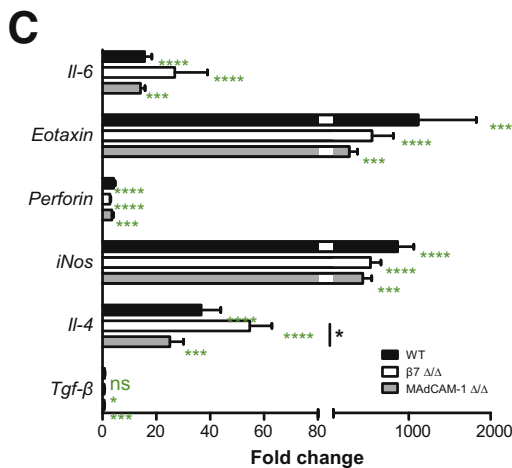
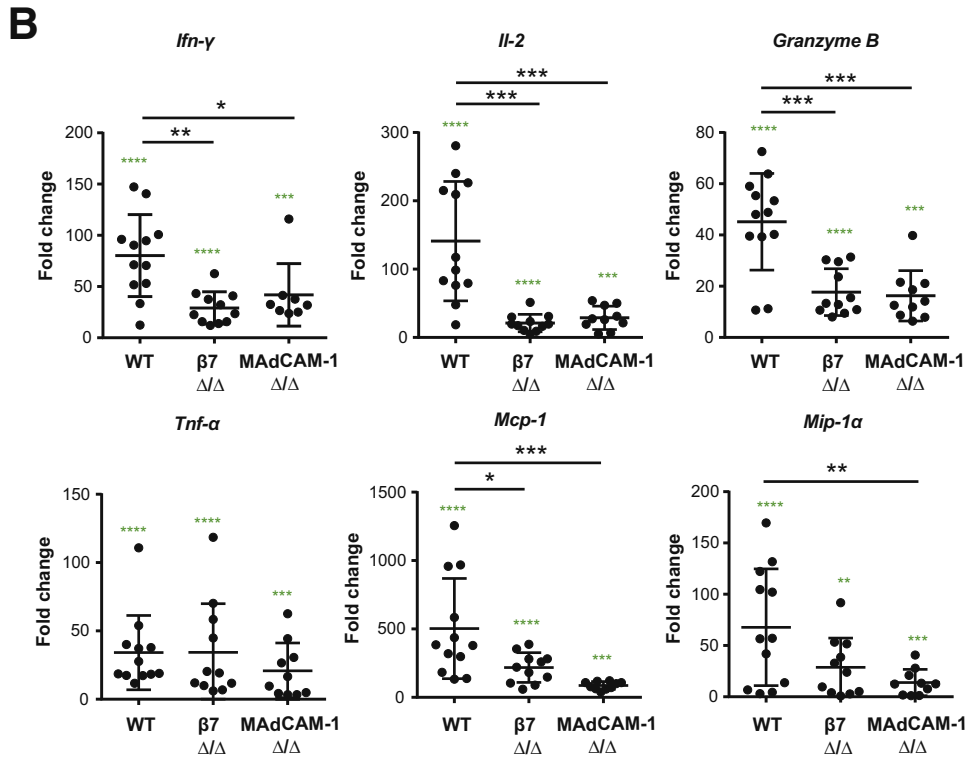
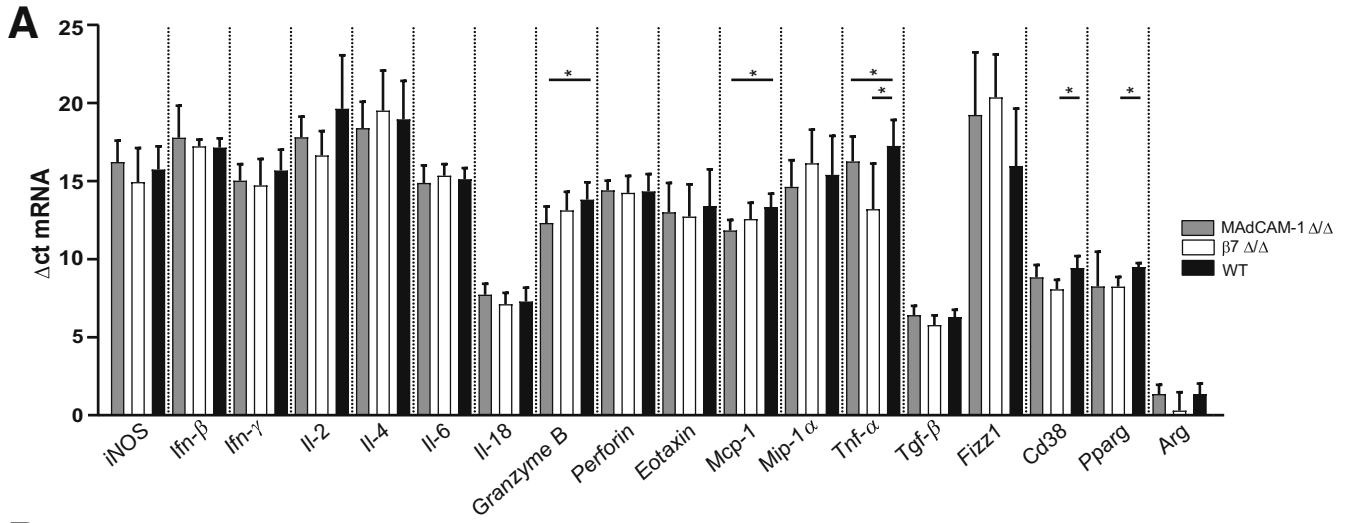


Figure 4. MAdCAM-1 expression is induced upon ConA treatment. (A) Levels of *Madcam-1* mRNA in liver tissue from WT mice at 0, 8, and 20 hours post ConA injection. Control (n = 5), 8 hours post-ConA (n = 7), 20 hours post-ConA (n = 7). mRNA levels are expressed as fold increase over the mean value obtained for healthy control liver tissue. (A) Data represent median with interquartile range and are representative of 3 independent experiments. Statistical significance was calculated by the Mann-Whitney nonparametric *t* test (**P* < .05, ***P* < .01). Statistical significance of deviation from healthy control animals for each mouse strain is shown as green asterisks above each group. (B) Cryostat sections of livers from the indicated mouse strains 8 or 20 hours after ConA administration or without were stained with anti-MAdCAM-1 antibody (green) and DAPI (blue) for visualization of nuclei. In addition, the central section on the right side was stained with anti-CD146 (red). Representative photomicrographs at original magnification $\times 40$. Scale bar = 100 μm .

immunofluorescence staining and real-time polymerase chain reaction (RT-PCR). Without ConA injection, we were unable to detect MAdCAM-1 expression in livers of WT mice (Figure 4A and B). However, 8 hours and 20 hours after ConA injection, positive MAdCAM-1 staining was

visible on vascular and sinusoidal endothelial cells. The vascular endothelial nature of MAdCAM-1-positive structures was confirmed by dual immunofluorescence staining with anti-MAdCAM-1 and anti-CD146 antibodies. No staining was detectable in ConA-treated MAdCAM-

Figure 3. (See previous page). MAdCAM-1- and $\beta 7$ integrin-deficient mice display reduced parameters of hemostasis following ConA treatment. Representative pictures of cryostat sections from WT livers 8 hours after ConA administration, which have been stained with (A) anti-PAI-1 antibody (green), anti-CD146 antibody (red), and DAPI (blue); (B) anti-TF antibody (red), β -catenin (green), and DAPI (blue); or (C) anti-CD41 (red), β -catenin (green), and DAPI (blue) and quantification as percentage of the fluorescently stained section area (n = 5 mice per group). Representative photomicrographs at original magnification $\times 40$. Scale bar = 100 μm . (A) mRNA levels of *Pai-1* (WT [n = 7], $\beta 7$ integrin Δ/Δ [n = 5], MAdCAM-1 Δ/Δ mice [n = 4]), and (B) *Tf* (WT [n = 7], $\beta 7$ integrin Δ/Δ [n = 4], MAdCAM-1 Δ/Δ mice [n = 3]) in liver tissue at 8 hours post-ConA injection. Values are expressed as fold increase over the mean values obtained for healthy control liver tissue from the respective mouse strain. Data show mean \pm SD. Statistical significance was calculated by the Mann-Whitney nonparametric *t* test **P* < .05, ***P* < .01; *****P* < .0001.



1-deficient mice (Figure 4B). In addition, we detected significantly increased *Madcam-1* mRNA levels in liver tissue homogenates of WT mice 8 and 20 hours after ConA challenge (Figure 4A).

MAdCAM-1 or $\beta 7$ Integrin Deficiency Reduces the Production of Proinflammatory Mediators

Subsequently, we investigated whether the observed attenuation of acute ConA-induced hepatitis was also reflected in changes in expression levels of cytokines and proinflammatory mediators in liver tissue homogenates. Between groups of untreated mice, none of the genes analyzed exhibited any obvious difference in levels of expression, indicating that no intrinsic leukocyte activation per se was caused by the loss of either MAdCAM-1 or $\beta 7$ integrin (Figure 5A, comparison of Δ ct values in homeostasis). In contrast, 8 hours following ConA administration, all mice showed a significant enhancement in hepatic mRNA levels for *Tnf- α* and *Ifn- γ* , the cytokines known to mediate ConA-induced liver damage. Moreover, *Il-2*, *granzyme B*, *Mcp-1*, and *Mip-1- α* , (Figure 5B) and *Il-4*, *Il-6*, *perforin*, *eotaxin*, and *iNos* (Figure 5C) were all significantly elevated in the ConA-treated mouse strains. Most importantly, $\beta 7$ integrin-deficient and MAdCAM-1-deficient mice exhibited a significantly reduced expression of the T cell-derived cytokines *Ifn- γ* and *Il-2* when compared with WT mice. In addition, MAdCAM-1-deficient mice showed a trend toward reduced expression of *Tnf- α* . Moreover, hepatic mRNA expression of the chemokines *Mip-1 α* and *Mcp-1* was reduced in $\beta 7$ integrin-deficient and MAdCAM-1-deficient mice. In addition, livers from mutant mice displayed a significant reduction in the expression of *granzyme b*, which is mainly derived from cytotoxic T lymphocytes and natural killer cells (Figure 5B). By contrast, there were no significant differences in the ConA-induced enhancement of *Il-4*, *Il-6*, *iNos*, *perforin*, *eotaxin*, and *Tgf- β* expression between WT and mutant mice (Figure 5C). In agreement with previous reports, expression levels of most inflammatory mediators had declined at 20 hours post-ConA injection, and differences between the different mouse strains were no longer significant (data not shown).

ConA-Mediated T Cell Accumulation and Activation in the Liver Is Not Disturbed in MAdCAM-1- and $\beta 7$ Integrin-Deficient Mice

In order to establish whether the reduced inflammatory response following ConA injury can be explained by reduced recruitment of lymphocytes to the liver, we investigated the effects of a lack of $\beta 7$ integrin or MAdCAM-1 on the composition of the immune cell population in the liver. Under steady state conditions, as evidenced by staining for the pan-leukocyte marker CD45 and quantification by flow cytometric analysis (gating strategy depicted in Figure 6), we detected a moderate increase in liver leukocyte numbers caused by MAdCAM-1 deficiency (MAdCAM-1 Δ/Δ : $0.8 \pm 0.0 \times 10^6$ cells/g liver; WT: $0.45 \pm 0.2 \times 10^6$ cells/g liver; $P < .05$), whereas liver leukocyte numbers from WT and $\beta 7$ integrin-deficient mice were comparable. Detailed analysis of major liver leukocyte groups, including lymphocytes, DCs, KCs, monocyte/macrophages, and M1/M2 macrophage subsets did not reveal any striking alterations in frequencies or polarization, caused by the adhesion molecule deficiency (Figure 7A–C).

Unfortunately, the preparation of liver cells from diseased mice is challenging in this model and the results very variable. The more the liver is affected and clotting occurs, the more difficult it becomes to flush the livers, resulting in lower cell numbers, especially in WT mice with the worst disease outcome. We therefore decided that a comparison of cellular frequencies would be the most objective measure. WT as well as $\beta 7$ integrin- and MAdCAM-1-deficient mice showed ConA-induced immune cell accumulation in the liver, but there was no significant difference in frequencies of intrahepatic leukocytes in the ConA-treated mice strains. Furthermore, the proportions of the different liver leukocyte subpopulations were comparable (Figure 7D and E).

ConA is a T cell mitogen that induces polyclonal T cell activation. Eight hours following ConA induction, all mice strains exhibited similar increases in the percentage of activated CD4⁺ and CD8⁺ T cells, as demonstrated by positive staining for the activation marker CD69, whereas the frequency of activated NK cells remained unchanged (Figure 8A).

Figure 5. (See previous page). MAdCAM-1- or $\beta 7$ integrin deficiency results in decreased production of ConA-induced proinflammatory mediators. Analysis of the mRNA of pro- and anti-inflammatory mediators in liver tissue from WT, $\beta 7$ integrin Δ/Δ , and MAdCAM-1 Δ/Δ mice by RT-PCR. Black bars represent data from WT, white bars from $\beta 7$ integrin Δ/Δ , and gray bars from MAdCAM-1 Δ/Δ mice: *Arg* (arginase), *Fizz1* (found in inflammatory zone 1), *Cd38* (cluster of differentiation 38), *Ifn* (interferon), *Il* (interleukin), *Mcp-1* (monocyte chemoattractant protein-1), *Mip-1 α* (macrophage inflammatory protein-1 α), *iNos* (inducible nitric oxide reductase), *Pparg* (peroxisome proliferator-activated receptor gamma), *Tgf- β* (tumor growth factor- β), *Tnf- α* (tumor necrosis factor- α). (A) Analysis in homeostasis. For quantification, values are expressed as delta (Δ) ct values between the genes of interest and the housekeeping gene *Gapdh* ($n = 4-9$). Data represent mean \pm SD. The statistical significance of variance between different genotypes was calculated by Mann-Whitney nonparametric t test ($*P < .05$). (B, C) Analysis 8 hours after ConA injection. For quantification, values are expressed as fold increase over the mean values obtained for control liver tissue from the respective untreated mouse strain. WT mice ($n = 12$), $\beta 7$ integrin Δ/Δ mice ($n = 10-11$), MAdCAM-1 Δ/Δ mice ($n = 8-10$). Data represent (B) mean \pm SD and (C) mean \pm SEM and are representative of 3 independent experiments. Statistical significance in panel B was calculated by the Mann-Whitney nonparametric t test and in panel C by 1-way analysis of variance with Tukey's multiple comparison posttest. Statistical significance of deviation from healthy control mice for each mouse strain is shown as green asterisks above each group and was calculated by the Mann-Whitney nonparametric t test ($*P < .05$, $**P < .01$, $***P < .001$, $****P < .0001$).

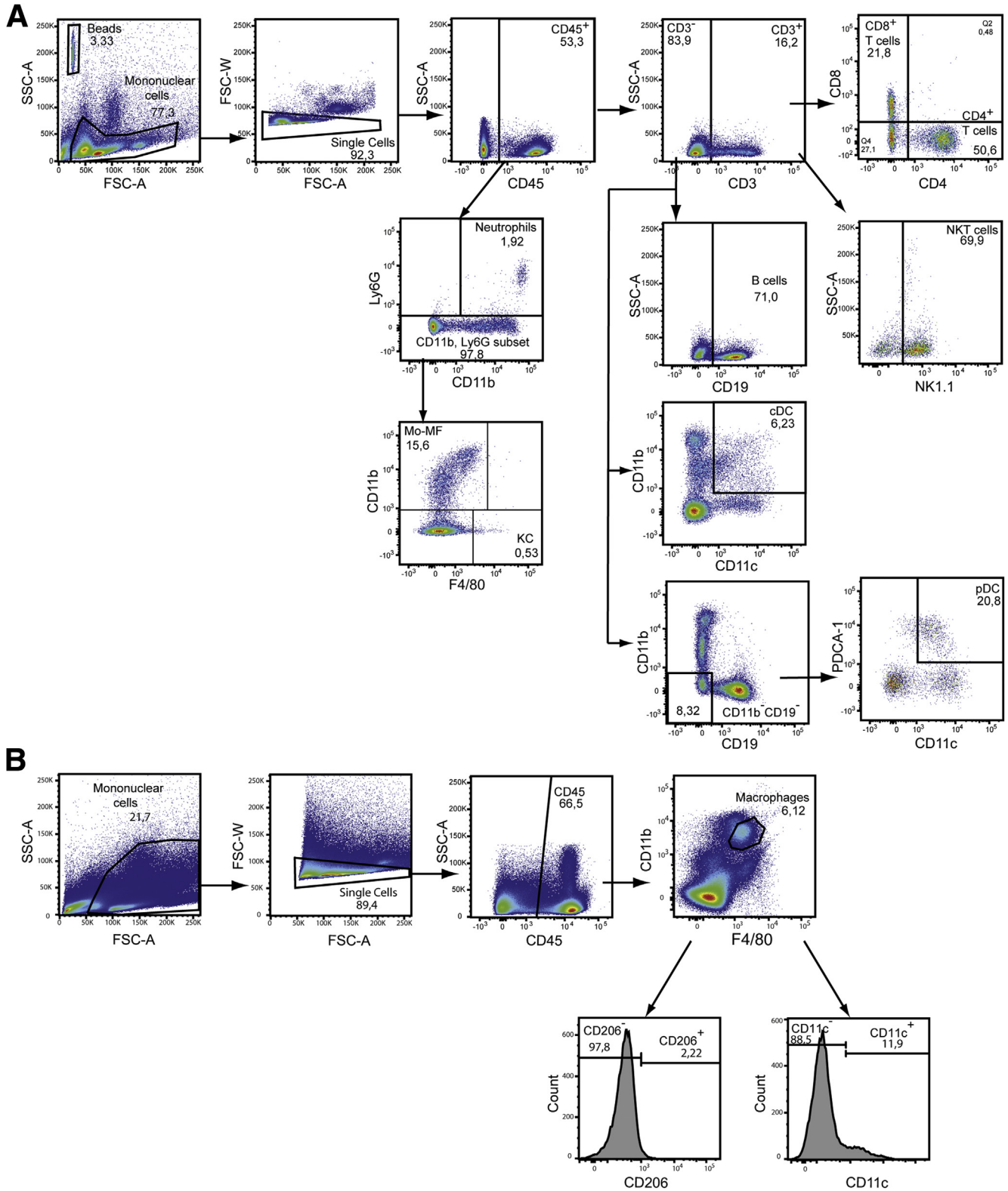
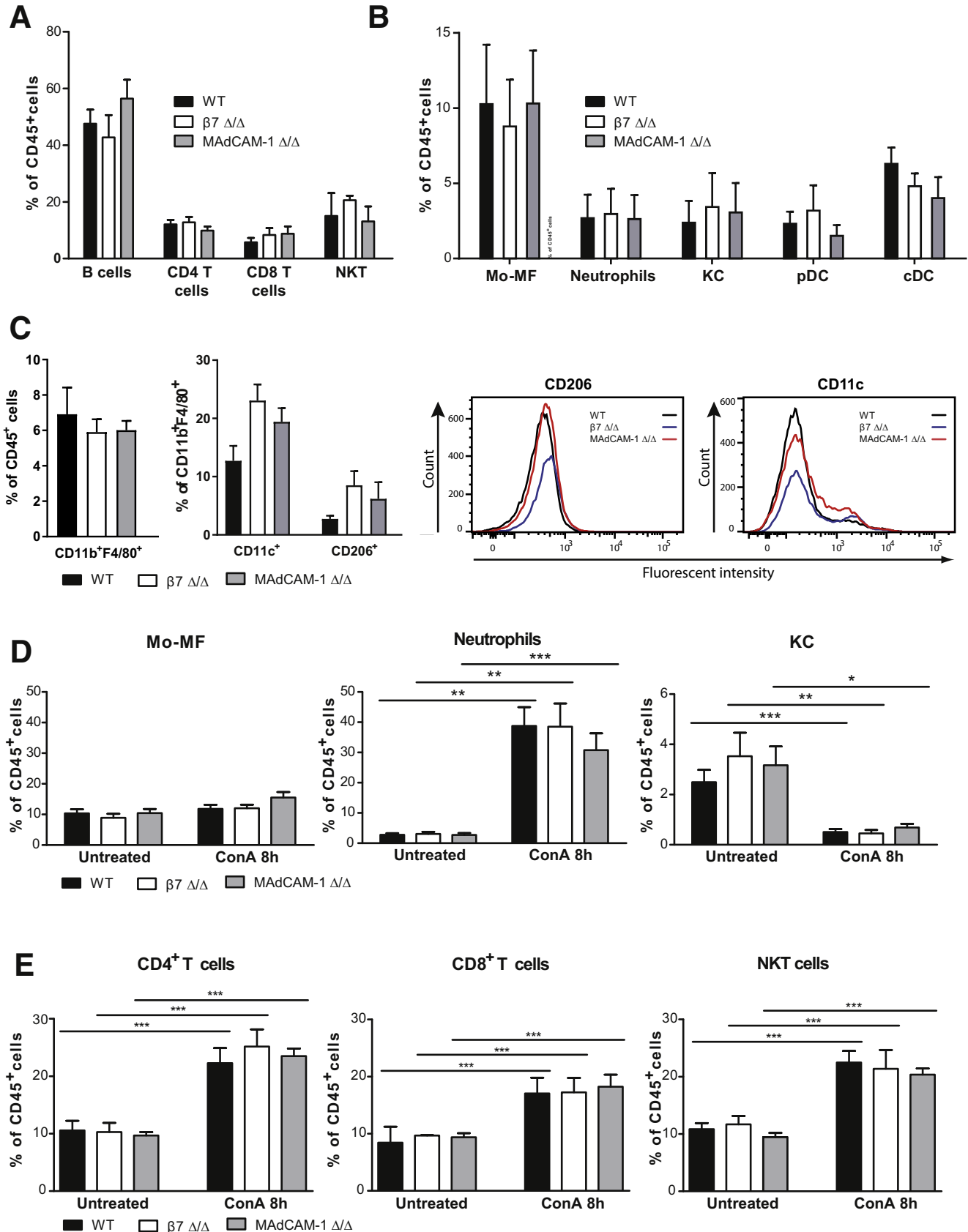


Figure 6. Immune cell subset gating strategies for liver cells by multiparameter flow cytometry. (A) General gating of liver cells. The analysis included B cells (CD45⁺CD3⁻CD19⁺), CD4⁺ T cells (CD45⁺CD3⁺CD4⁺), CD8⁺ T cells (CD45⁺CD3⁺CD8⁺), NKT cells (CD45⁺CD3⁺NK1.1⁺), monocytes/macrophages (Mo-MF) (CD45⁺CD11b⁺Ly6G⁻F4/80⁺), neutrophils (CD45⁺CD11b⁺Ly6G⁺), KCs (CD45⁺CD11b⁻Ly6G⁺F4/80⁺), plasmacytoid DCs (pDCs) (CD45⁺CD3⁻CD19⁻CD11c⁺PDCA1⁺), and conventional DCs (cDCs) (CD45⁺CD3⁻CD11c⁺CD11b⁺). (B) M1/M2 differentiation. The analysis included M1 macrophages (CD45⁺CD11b⁺F4/80⁺CD11c⁺) and M2 macrophages (CD45⁺CD11b⁺F4/80⁺CD206⁺).

We have also tested the different leukocyte subpopulations from the liver of WT mice for the expression of $\beta 7$ integrin. In homeostasis, only 15% of the CD4⁺ T cells

express $\beta 7$ integrin, whereas this adhesion molecule is expressed on about 20% of NKT cells and on more than 50% of CD8⁺ T cells (Figure 8B and C). Interestingly, ConA



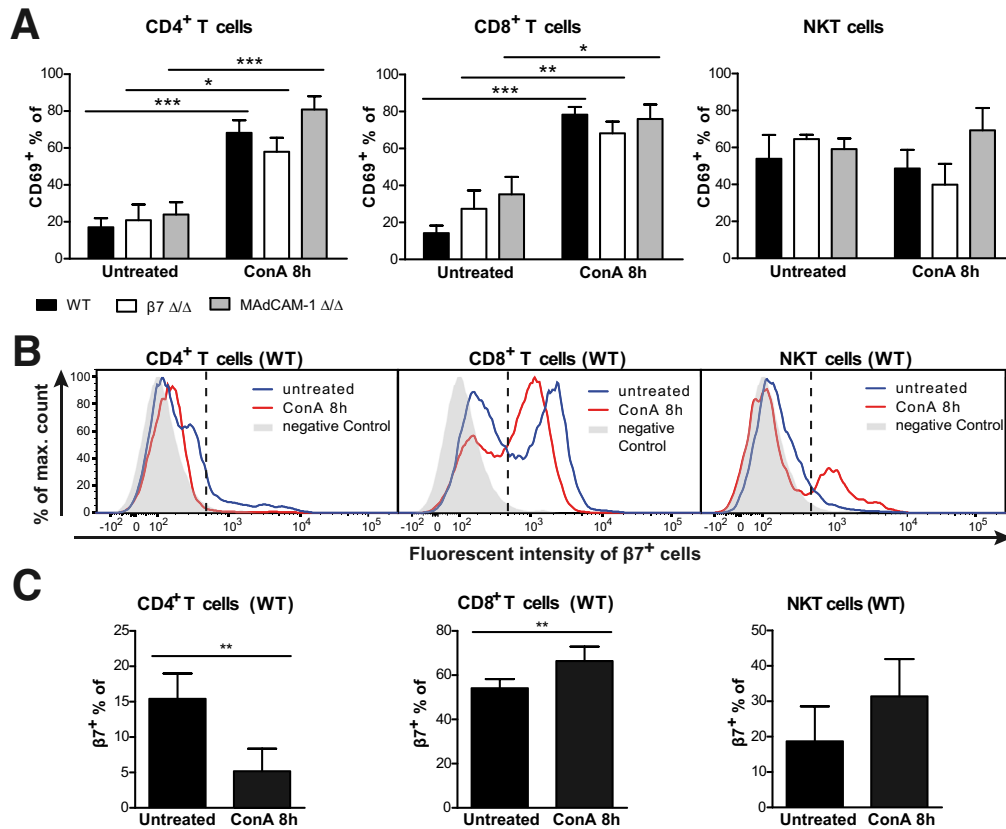


Figure 8. MAdCAM-1- and $\beta 7$ integrin-deficient mice display similar levels of ConA-mediated T cell activation. Eight hours after ConA treatment, total leukocytes were isolated from livers and analyzed by flow cytometry. Representative FACS dot plots illustrating the gating strategy are shown in Figure 6. Data represent (A) mean \pm SEM and (C) mean \pm SD and are representative of 3 independent experiments. Statistical significance was calculated by the Mann-Whitney nonparametric *t* test (**P* < .05, ***P* < .001, ****P* < .001). (A) Percentages of activated CD4⁺T (CD45⁺CD3⁺CD4⁺CD69⁺), CD8⁺T (CD45⁺CD3⁺CD4⁺CD69⁺), and NKT (CD45⁺CD3⁺NK1.1⁺CD69⁺) cells were quantified. WT (black bars, n = 7–9), $\beta 7$ integrin Δ/Δ (white bars, n = 5–7), and MAdCAM-1 Δ/Δ mice (gray bars, n = 5–7). (B, C) ConA-mediated shift in the percentage of $\beta 7$ integrin-positive cells in WT mice: (B) as percent of the maximal cell count for the indicated cells populations and (C) as percent of cells expressing $\beta 7$ integrin within the indicated cell populations. Untreated WT (n = 5) ConA-treated WT (n = 10).

challenge causes a shift in the percentage of $\beta 7$ integrin-expressing cells with a decrease among the CD4⁺ T cells, whereas the percentage of $\beta 7$ integrin-expressing cells among the CD8⁺ T cells and NKT cells is increased. Considering the percentage of $\beta 7$ integrin-positive cells among activated CD69⁺ cells, this shift is even more

pronounced, with a ConA-induced increase from 30% to 70% among the CD69⁺CD8⁺ T cells and from 15% to 30% among the CD69⁺NKT cells (Figure 9A and B). Regarding the other immune cells, ConA treatment did not cause any significant increase in $\beta 7$ integrin expression on monocytes/macrophages, neutrophils, plasmacytoid DCs, and

Figure 7. (See previous page). Comparative liver analysis of WT, $\beta 7$ integrin Δ/Δ , and MAdCAM-1 Δ/Δ mice in homeostasis and following ConA treatment. (A–C) Total leukocytes were isolated from livers of WT (black bars), $\beta 7$ integrin Δ/Δ (white bars), and MAdCAM-1 Δ/Δ (gray bars) mice in homeostasis, or (D, E) also 8 hours after ConA injection, followed by flow cytometric quantification of leukocytes. Representative FACS (fluorescence-activated cell sorting) dot plots illustrating the gating strategy are shown in Figure 6. B cells (CD45⁺CD3[−]CD19⁺), CD4⁺ T cells (CD45⁺CD3⁺CD4⁺), CD8⁺ T cells (CD45⁺CD3⁺CD8⁺), NKT cells (CD45⁺CD3⁺NK1.1⁺), Mo-MF (CD45⁺CD11b⁺Ly6G[−]F4/80⁺), neutrophils (CD45⁺CD11b⁺Ly6G⁺), KCs (CD45⁺CD11b[−]Ly6G[−]F4/80⁺), pDCs (CD45⁺CD3[−]CD19[−]CD11c⁺PDCA1⁺), cDCs (CD45⁺CD3[−]CD11c⁺CD11b⁺), macrophages (CD45⁺CD11b⁺F4/80⁺), M1 macrophages (CD45⁺CD11b⁺F4/80⁺CD11c⁺), and M2 macrophages (CD45⁺CD11b⁺F4/80⁺CD206⁺). Cells are shown as percent of CD45⁺ cells or percent of CD45⁺CD11b⁺F4/80⁺ cells as indicated. Data represent (A–C) mean \pm SD and (D, E) mean \pm SEM and are representative of (C) 2 or (A, B, D, E) 3 independent experiments. Representative overlay histograms at the right side of panel C show that there is no difference in CD11c and CD206 staining intensity on CD11b⁺F4/80⁺ liver macrophages from WT, $\beta 7$ integrin Δ/Δ , and MAdCAM-1 Δ/Δ mice. Statistical significance was calculated by the Mann-Whitney nonparametric *t* test and is indicated by the following symbols: **P* < .05, ***P* < .01, ****P* < .001. (A, B) WT, n = 10; $\beta 7$ integrin Δ/Δ , n = 10; MAdCAM-1 Δ/Δ , n = 10. (C) WT, n = 3; $\beta 7$ integrin Δ/Δ , n = 3; MAdCAM-1 Δ/Δ , n = 3. (D) WT, n = 9–13; $\beta 7$ integrin Δ/Δ , n = 6–11; MAdCAM-1 Δ/Δ , n = 7–10. (E) WT, n = 9–13; $\beta 7$ integrin Δ/Δ , n = 5–11; MAdCAM-1 Δ/Δ , n = 5–10.

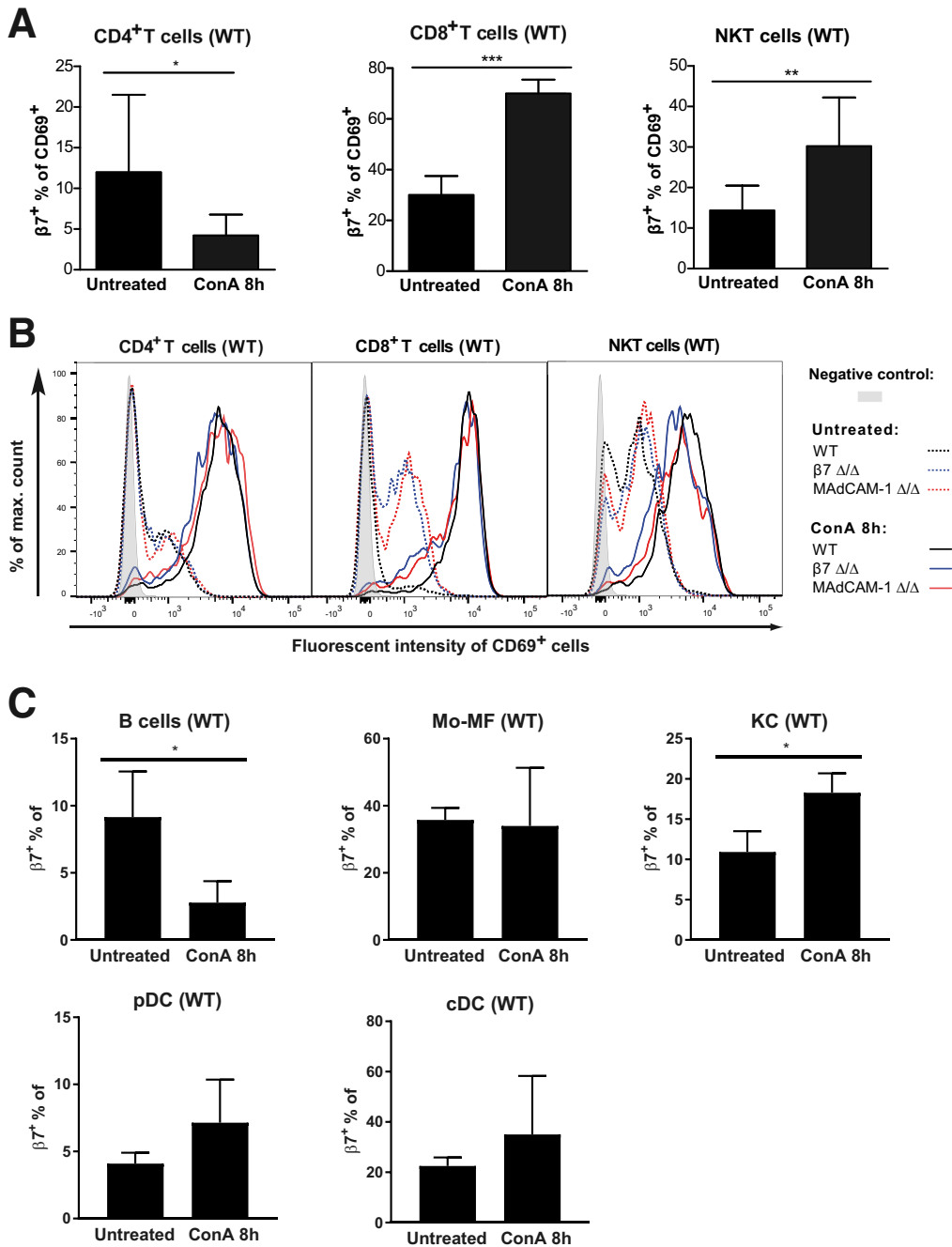


Figure 9. ConA-mediated shift in the percentage of $\beta 7$ integrin-positive cell populations in livers of WT mice. Eight hours after ConA treatment, total leukocytes were isolated from livers and analyzed by flow cytometry. Representative FACS dot plots illustrating the gating strategy are shown in Figure 6. Data represent mean \pm SD. Statistical significance was calculated by the Mann-Whitney nonparametric *t* test (**P* < .05, ***P* < .001, ****P* < .001). (A) ConA-mediated shift in the percentage of $\beta 7$ integrin-positive cells in WT mice as percent of activated CD69⁺ cells expressing $\beta 7$ integrin within the CD4⁺T (CD45⁺CD3⁺CD4⁺CD69⁺), CD8⁺T (CD45⁺CD3⁺CD4⁺CD69⁺), and NKT (CD45⁺CD3⁺NK1.1⁺CD69⁺) cells. Untreated WT (n = 5) ConA-treated WT (n = 10). (B) Representative histograms illustrating percent of the maximal cell count for activated CD69⁺ CD4⁺ T cells, CD69⁺ CD8⁺ T cells, and CD69⁺ NKT cells for the different mouse mutants as indicated. (C) ConA-mediated shift in the percentage of $\beta 7$ integrin-positive cells in WT mice as percent of cells expressing $\beta 7$ integrin within the indicated cell populations. Untreated WT (n = 4), ConA-treated WT (n = 6).

conventional DCs, whereas on B cells the expression was downregulated to a certain degree. Only for KCs did we detect a small but significant increase (Figure 9C).

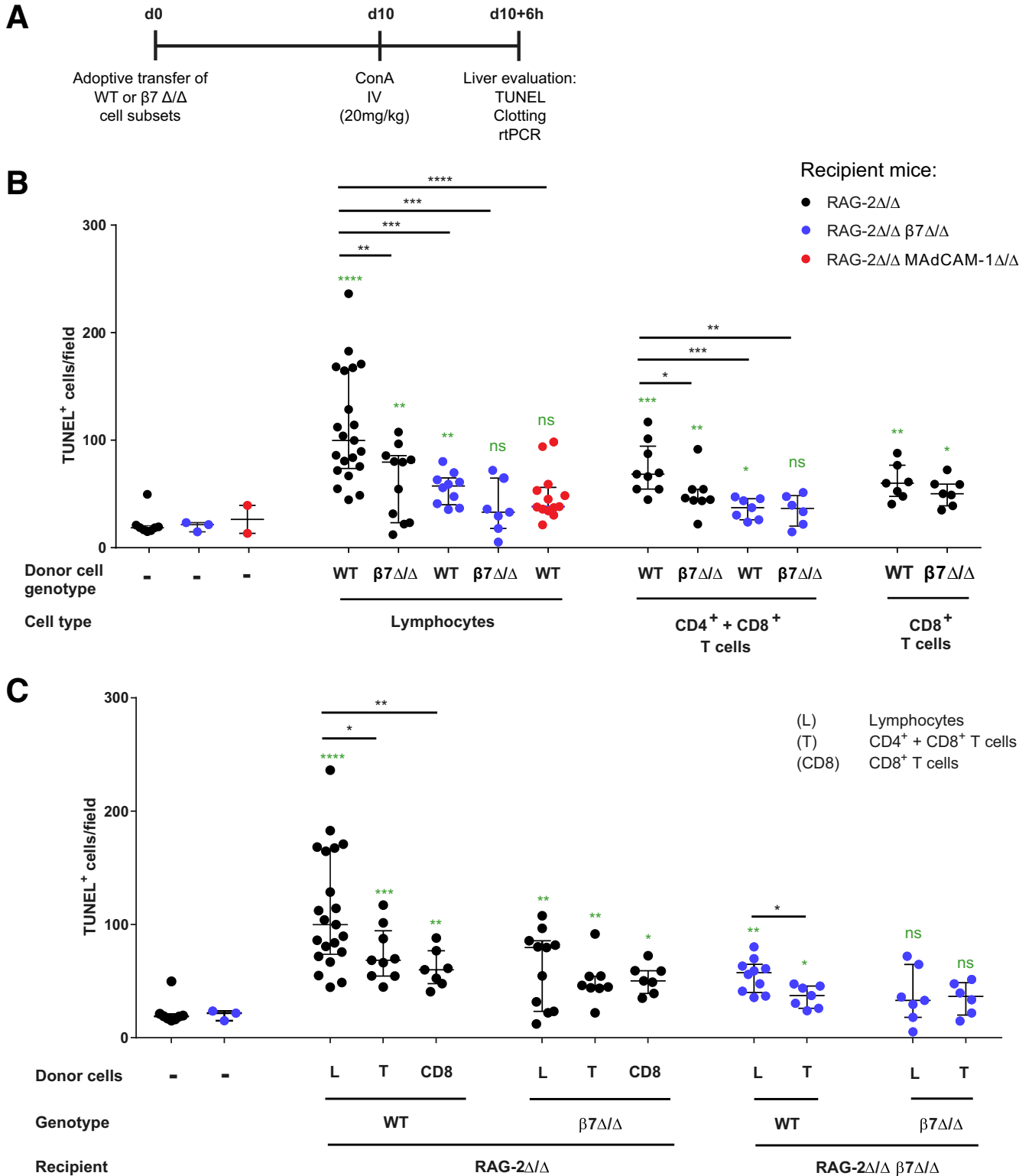
Expression of $\beta 7$ Integrin on Adaptive and Innate Immune Cells Contributes to ConA-Mediated Liver Damage and Is Crucial for ConA-Induced MAdCAM-1 Expression

In addition to CD4⁺ T cells, which have been described as the main effector cells driving ConA-induced hepatitis,

CD8⁺ T cells, NKT cells, neutrophils, macrophages, and KCs seem to be involved in ConA-mediated liver damage.^{1,4,23} The observed ConA-induced increase in the percentage of $\beta 7$ integrin-expressing activated CD8⁺ T cells and NK cells suggests that these cells contribute to the destructive process. To address this question, we used RAG-2-deficient mice, which lack mature T and B cells, to study the impact of different subsets of lymphocytes on ConA-mediated liver damage by means of cell transfer experiments (Figure 10A). To this end, we isolated lymphocytes, or a mixture of CD4⁺ and CD8⁺ T cells, or CD8⁺ T cells only, from lymph nodes of WT or $\beta 7$ integrin-deficient mice. These cells were then

intravenously transferred into RAG-2 deficient, RAG-2/ $\beta 7$ integrin double-deficient, or RAG-2/MAdCAM-1 double-deficient recipient mice, 10 days prior to ConA injection. Animals without a functional T lymphocyte compartment are not susceptible to ConA, as T cell activation is a crucial

factor in this model of liver damage.^{1,24} As expected, without cell transfer, none of the RAG-2-deficient or double-deficient mice developed liver damage, as demonstrated by TUNEL staining 6 hours after ConA injection. In contrast, a significant increase in TUNEL-positive cells was detected



in the livers of all RAG-2-deficient recipients and all RAG-2/ $\beta 7$ integrin double-deficient recipients of WT lymphocytes or WT CD4⁺/CD8⁺ T cell mixtures, though the extent of this increase varied. Interestingly, RAG-2/ $\beta 7$ integrin double-deficient recipients of $\beta 7$ integrin-deficient lymphocytes or $\beta 7$ integrin-deficient CD4⁺/CD8⁺ T cell mixtures, and RAG-2/MAdCAM-1 double-deficient recipients of WT lymphocytes were protected from apoptosis (Figure 10B). Reconstitution of RAG-2-deficient mice with WT lymphocytes or WT CD4⁺/CD8⁺ T cell mixtures led to significantly higher numbers of apoptotic cells compared with reconstitution of these mice with $\beta 7$ integrin-deficient lymphocytes or $\beta 7$ integrin-deficient CD4⁺/CD8⁺ T cell mixtures, respectively, pointing to the importance of lymphocytic $\beta 7$ integrin in the destructive process. Remarkably, reconstitution of RAG-2/ $\beta 7$ integrin double-deficient mice with WT lymphocytes or WT CD4⁺/CD8⁺ T cell mixtures, resulted in less apoptosis than reconstitution of RAG-2 mice with the respective cells sets, indicating a contribution of $\beta 7$ integrin-expressing innate immune cells to the destructive process. Exclusive transfer of WT or $\beta 7$ integrin-deficient CD8⁺ T cells into RAG-2-deficient mice caused only a small increase in apoptosis with no difference in genotype between the transferred cells, thus pointing to the minor contribution of CD8⁺ T cells in this model, which is independent of $\beta 7$ integrin. In addition, independent of the genotype of the transferred cells, we noticed a gradual decrease in liver damage when transferring whole lymphocytes, CD4⁺/CD8⁺ T cell mixtures, or CD8⁺ T cells only, suggesting a potential contribution of further cell types such as B cells or NKT cells (Figure 10C).

Hepatic platelet aggregation contributes to ConA-induced liver damage²⁵ and was much less prominent in the livers of MAdCAM-1- or in $\beta 7$ integrin-deficient mice. Therefore, we evaluated the impact of the different lymphocyte subsets on ConA-mediated liver damage by quantifying the area of cell clotting on the liver sections. Here, our results broadly mirror the findings of the TUNEL evaluation, with no ConA-induced clotting in mice without cell transfer and significantly reduced clotting after cell transfer in RAG-2/ $\beta 7$ integrin double-deficient mice and RAG-2/MAdCAM-1 double-deficient mice when compared with RAG-2-deficient mice. This suggests that $\beta 7$ integrin-expressing innate immune cells contribute to cell clotting (Figure 11A). In addition, we observed a gradual decrease in clotting when transferring whole lymphocytes or CD4⁺/CD8⁺ T cell mixtures (Figure 11B). In contrast, no

clotting was observed upon transfer of CD8⁺ T cells only and we did not detect any difference in clotting based on the genotype of the cell type transferred (WT or $\beta 7\Delta/\Delta$), which suggests that clotting in this experimental system is independent of CD8⁺ T cells and the expression of $\beta 7$ integrin on lymphocytes.

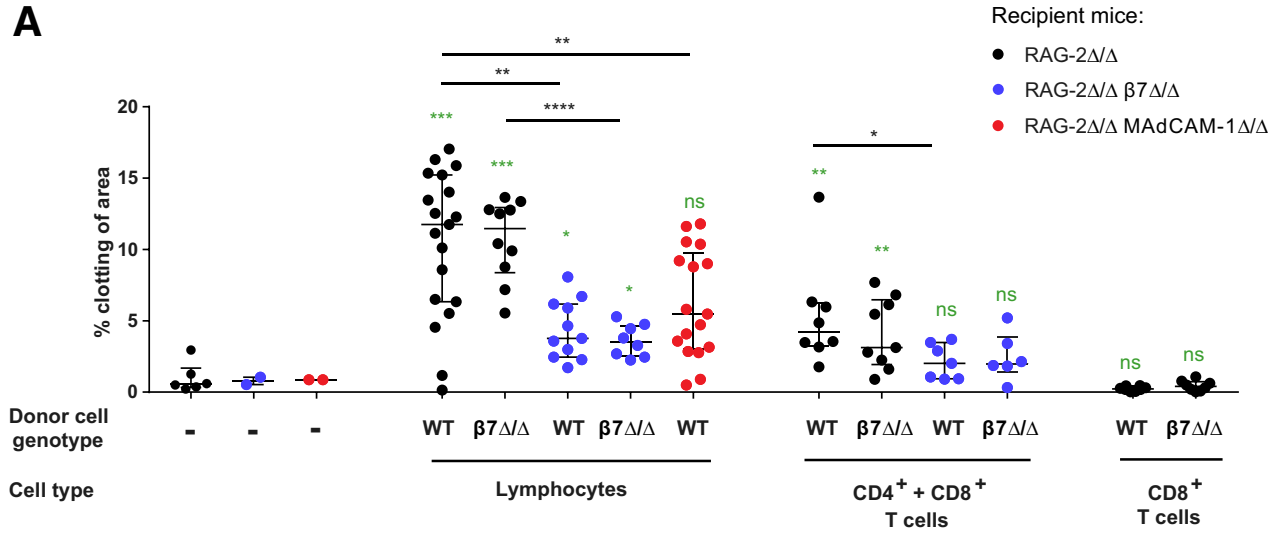
Moreover, we analyzed the expression of *Madcam-1* mRNA in liver tissue homogenates of RAG-2-deficient mice to which ConA-treated lymphocytes had been transferred and similarly treated RAG-2/ $\beta 7$ integrin double-deficient mice or RAG-2/MAdCAM-1 double-deficient mice. In addition, we performed immunofluorescence stainings on liver sections of the respective mice. Interestingly, neither non-treated RAG-2-deficient mice, nor RAG-2-deficient mice that had received $\beta 7$ integrin-deficient lymphocytes or RAG-2/ $\beta 7$ integrin double-deficient mice that had received WT lymphocytes exhibited an elevated *Madcam-1* mRNA level. Only after WT lymphocyte transfer did RAG-2-deficient mice show increased *Madcam-1* mRNA and positive staining for MAdCAM-1, suggesting that $\beta 7$ integrin expression on innate and adaptive immune cells is crucial for the induction of MAdCAM-1 (Figure 11C and D).

Lymphocyte Adhesion to Liver Sinusoid Endothelium Depends on MAdCAM-1

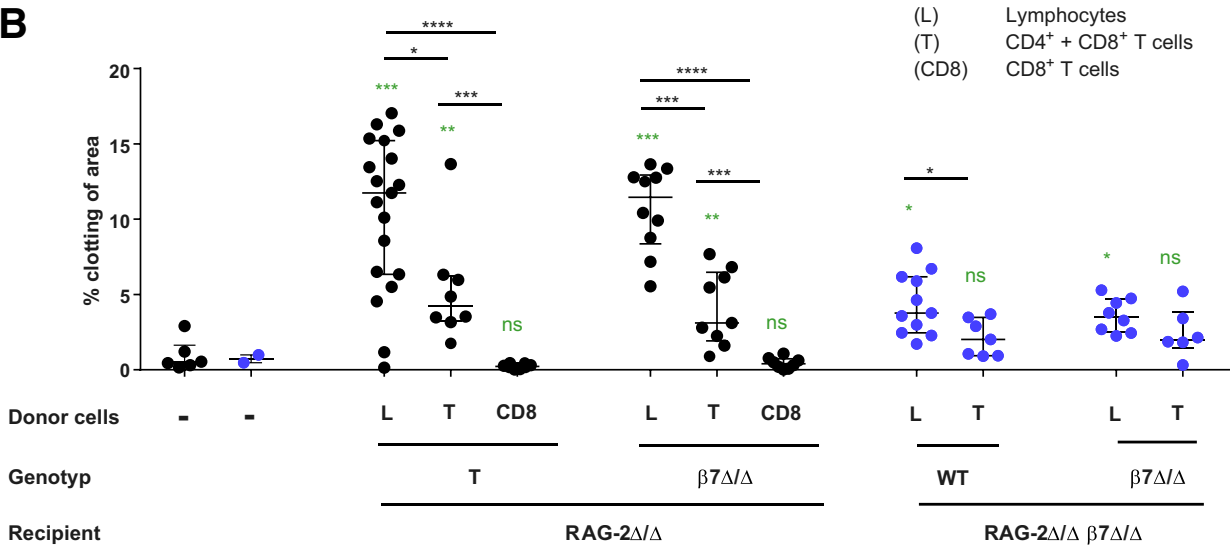
To assess the effect of a disrupted $\beta 7$ integrin/MAdCAM-1 interaction on leukocyte migratory behavior during the pathogenesis of ConA-mediated liver damage, we performed intravital 2-photon laser scanning microscopy in livers of MAdCAM-1 Δ/Δ /CX3CR1^{+eGFP} mice and CX3CR1^{+eGFP} control mice.²⁶ CX3CR1^{+eGFP} mice were utilized as recipients, since in these mice circulating monocytes and liver resident DCs are made visible by GFP expression. Mice were intravenously injected with whole lymphocyte suspensions, as these had previously resulted in the most prominent liver damage on ConA administration. Lymphocyte suspensions were isolated from DsRed mice²⁷ and contained at least 70% T cells, as confirmed by flow cytometry (Figure 12A). They exhibited red fluorescence, allowing us to visualize monocytes (GFP⁺) and lymphocytes (DsRed⁺) in the liver in vivo and to distinguish between motile and stationary cells. Livers were first imaged under baseline conditions to exclude preparation-dependent artifacts in blood flow and cell migration (not shown). ConA was then administered by intracardiac injection, and cellular migration was monitored over a time period of around 2 hours.

Figure 10. (See previous page). **Expression of $\beta 7$ integrin on adaptive and innate immune cells contributes to ConA-mediated liver damage.** (A) Experimental outline: RAG-2-deficient (RAG-2 Δ/Δ), RAG-2/ $\beta 7$ integrin double-deficient (RAG-2 Δ/Δ $\beta 7\Delta/\Delta$), and RAG-2/MAdCAM-1 double-deficient (RAG-2 Δ/Δ MAdCAM-1 Δ/Δ) mice were adoptively transferred with WT or $\beta 7\Delta/\Delta$ cell subsets (lymphocytes, CD4⁺ and CD8⁺ T cells, CD8⁺ T cells, or no cells) and after 10 days subjected to ConA by intravenous tail injection. Six hours later, liver specimens were sampled and analyzed. Black symbols represent RAG-2 Δ/Δ , blue symbols represent RAG-2 Δ/Δ $\beta 7\Delta/\Delta$, and red symbols represent RAG-2 Δ/Δ MAdCAM-1 Δ/Δ recipient mice. Data are represented as median with interquartile range and statistical significance was calculated by the Mann-Whitney nonparametric *t* test. Statistical significance of deviation from ConA-treated control mice (without cell transfer) for each mouse strain is shown as green asterisks above each group. **P* < .05, ***P* < .01, ****P* < .001, *****P* < .0001. (B) Quantification of apoptotic cells as detected by TUNEL assay in liver sections (n \geq 6 mice per group); direct comparison of the indicated recipients. (C) Quantification of apoptotic cells as detected by TUNEL assay in liver sections (n \geq 6 mice per group); direct comparison of the indicated donor cell populations.

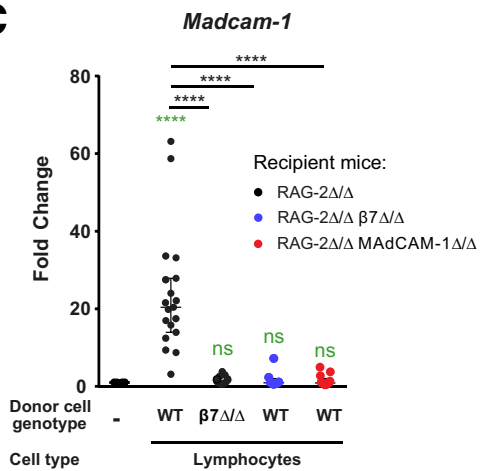
A



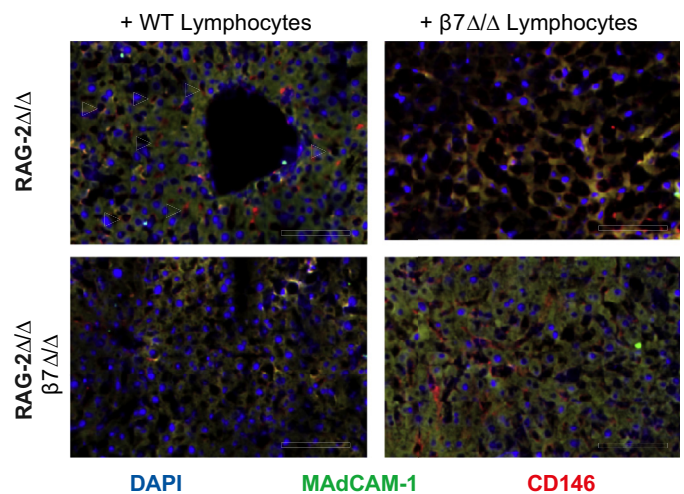
B



C



D



Administration of ConA leads to a rapid loss of cellular motility within the first 30 minutes following injection, causing an almost complete arrest of the lymphocytes within the liver sinusoids of CX3CR1^{+/eGFP} control mice. By contrast, DsRed⁺ lymphocytes injected into MAdCAM-1Δ/Δ/CX3CR1^{+/eGFP} mice exhibited increased motility compared with DsRed⁺ lymphocytes injected into CX3CR1^{+/eGFP} control animals. Notably, this was manifested in an increased displacement and track length, an increased individual cell speed, and average track speed as well as a decreased number of static cells (Figure 12B–H and Supplementary Videos 1 and 2). Accumulation of DsRed-labeled cells, independent of the genotype of the recipient mice, was found in periportal rather than pericentral areas (representative images are depicted in Figure 12I). However, in line with the overall image analysis, cells were trapped in place more efficiently in CX3CR1^{+/eGFP} control animals than in MAdCAM-1Δ/Δ/CX3CR1^{+/eGFP} mice. Collectively, these data provide evidence that ConA induces MAdCAM-1-dependent interactions between lymphocytes and endothelial liver cells.

Discussion

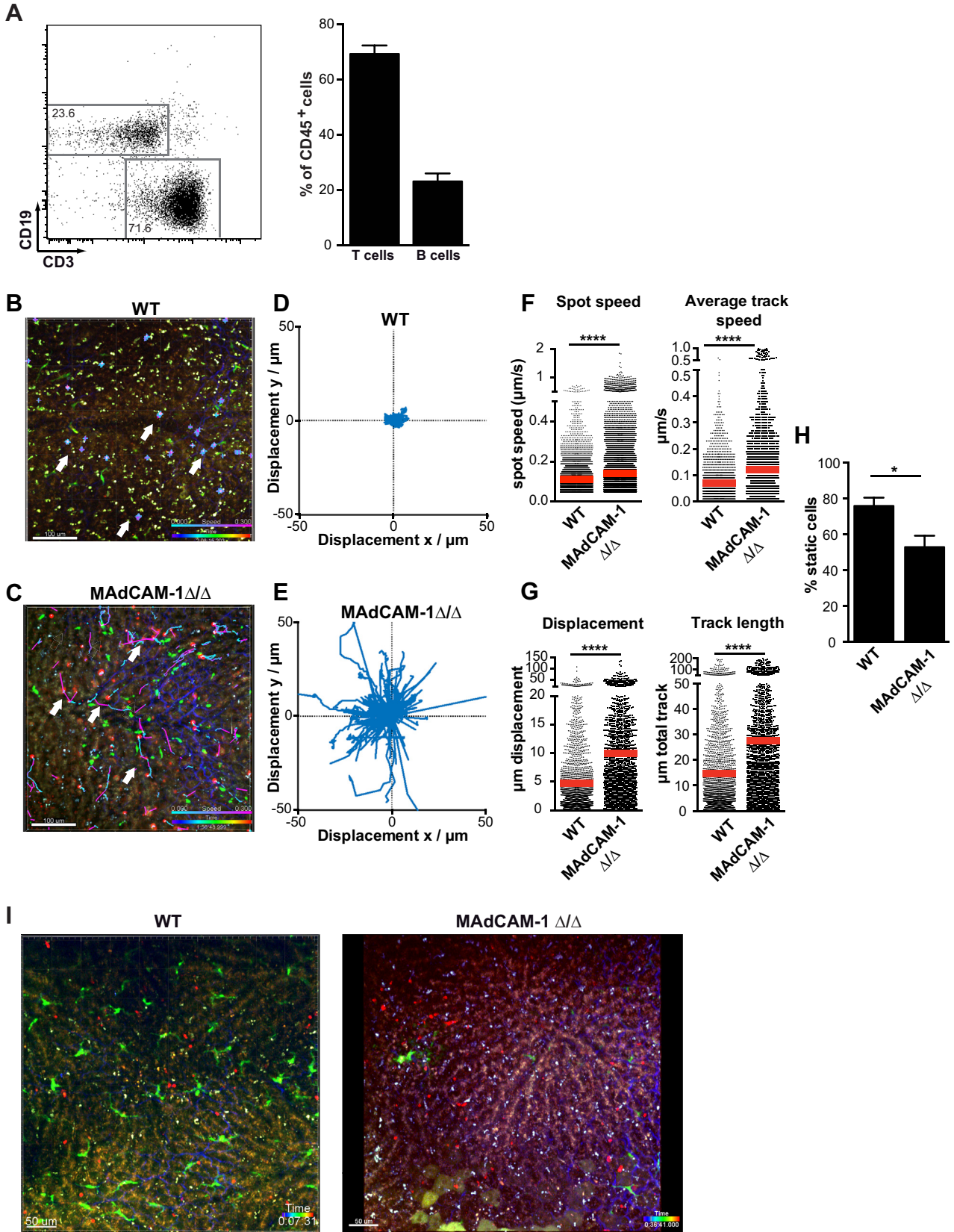
Integrin-mediated leukocyte recruitment has been shown to contribute to diseases as diverse as multiple sclerosis and IBD. Besides, clinical trials have demonstrated that immunoneutralizing α4 integrin with natalizumab or α4β7 integrin with vedolizumab significantly improves multiple sclerosis or IBD, respectively.^{28,29} We set up experiments to elucidate the role of the leukocyte adhesion molecule β7 integrin and its endothelial ligand MAdCAM-1 in acute immune-mediated liver inflammation.

Hepatic injury in the well-established ConA-induced hepatitis model is associated with leukocyte infiltration and CD4⁺ T cells and NKT cells, in particular, have been identified as effector cells in this model of hepatitis. MAdCAM-1- and β7 integrin-deficient mice were markedly protected from ConA-induced liver injuries. They exhibited decreased levels of liver aminotransferases and diminished liver necrosis and apoptosis. The formation of hemorrhagic lesions

was also significantly reduced. Moreover, we detected a reduced expression of proinflammatory mediators such as *Ifn-γ*, *Il-2*, *Mip-1α*, and *Tnf-α* and of T cell effector molecules such as *granzyme B* in liver tissue of ConA-treated mutant mice. As neutralization of *Tnf-α* or *Ifn-γ* protects mice from ConA-induced hepatitis,^{2–4} these 2 cytokines are regarded as essential for the development of ConA hepatitis. Interestingly, we could not identify any differences in the ConA-induced overall accumulation of leukocytes and of T cell activation between livers of WT and β7 integrin-deficient or MAdCAM-1-deficient mice. Of course, our analysis is not detailed enough to reveal potential differences in specific T cell subsets (eg, regulatory T cells), which might not affect total T cell numbers. In addition, the damage to the liver in this model develops extremely fast, within hours, and may at this early stage not be critically dependent on immune cell infiltration of the liver parenchyma.

To our knowledge, we are the first to have shown, by in vivo 2-photon microscopy, an increase in the firm adhesion of lymphocytes in the liver sinusoids of WT mice within 30 minutes of ConA administration, and a marked reduction of this lymphocyte binding in the liver tissue of MAdCAM-1-deficient mice. Therefore, most probably, MAdCAM-1-dependent interactions between lymphocytes and endothelial liver cells are critically involved in ConA-induced hepatitis, as evidenced by the amelioration of the hepatitis upon inhibition of MAdCAM-1. β7 integrin expression was clearly detectable on a population of T cells and NKT cells in the liver of untreated mice. This most likely contributes to the increased firm adhesion of lymphocytes observed in the liver of WT mice within the first 30 minutes following ConA administration. The firm adhesion of lymphocytes to sinusoidal epithelium occurring 30 minutes after ConA administration is too fast to be explained by newly synthesized MAdCAM-1 molecules in WT mice. One possible scenario is that the ConA-induced inflammatory signaling causes a structural change or redistribution of already existing MAdCAM-1 molecules onto the cell surface, thereby leading to a functional conformation that allows lymphocyte-integrin recognition and binding. Such cell surface redistribution of MAdCAM-1 protein has already

Figure 11. (See previous page). Expression of β7 integrin on adaptive and innate immune cells contributes to ConA-mediated clotting and is crucial for ConA-induced MAdCAM-1 expression. RAG-2-deficient (RAG-2Δ/Δ), RAG-2/β7 integrin double-deficient (RAG-2Δ/Δ β7Δ/Δ), and RAG-2/MAdCAM-1 double-deficient (RAG-2Δ/Δ MAdCAM-1Δ/Δ) mice were adoptively transferred with WT or β7Δ/Δ cell subsets (lymphocytes, CD4⁺ and CD8⁺ T cells, CD8⁺ T cells, or no cells) and after 10 days subjected to ConA by intravenous tail injection. Six hours later, liver specimens were sampled and analyzed. Black symbols represent RAG-2Δ/Δ, blue symbols represent RAG-2Δ/Δ β7Δ/Δ, and red symbols represent RAG-2Δ/Δ MAdCAM-1Δ/Δ recipient mice. Data are represented as median with interquartile range and statistical significance was calculated by the Mann-Whitney nonparametric *t* test. Statistical significance of deviation from ConA-treated control mice (without cell transfer) for each mouse strain is shown as green asterisks above each group. **P* < .05, ***P* < .01, ****P* < .001, *****P* < .0001. (A) Quantification of clotting in H&E-stained liver sections shown as percentage of the section area (n ≥ 6 mice per group); direct comparison of the indicated recipients. (B) Quantification of clotting in H&E-stained liver sections shown as percentage of the section area (n ≥ 6 mice per group); direct comparison of the indicated donor cell populations. (C) mRNA levels of *Madcam-1* in liver tissue. Values are expressed as fold increase over the mean value obtained for the different ConA-treated recipient mice without cell transfer (n ≥ 6 per group). (D) Cryostat sections of livers from ConA-treated RAG-1Δ/Δ or RAG-2Δ/Δβ7Δ/Δ mice, which had been adoptively transferred with WT or β7Δ/Δ lymphocytes as indicated, were stained with anti-MAdCAM-1 antibody (green), anti-CD146 antibody (red), and DAPI (blue) for visualization of nuclei. MAdCAM-1/CD146 double-staining in sinusoids is marked by white arrowheads. Representative photomicrographs at original magnification ×40. Scale bar = 100 μm.



been demonstrated *in vitro* after stimulation of human hepatic endothelial cells with tumor necrosis factor α and methylamine.³⁰

ConA administration induces prominent intrasinusoidal clotting. The consequence is a marked deceleration of intrahepatic blood flow and elevation of portal perfusion pressure, followed by confluent hepatic necrosis within the congested area of liver parenchyma.²¹ Hepatic platelet aggregation contributes to ConA-induced hepatitis,²⁵ and in MAdCAM-1- and $\beta 7$ integrin-deficient mice ConA-induced hemostasis was much less pronounced. Moreover, these mice exhibited a reduction in the hepatic mRNA expression of *Tf* and *Pai-1*, factors initiating blood coagulation and inhibiting fibrinolysis, respectively. Expression of both factors is accomplished to some extent by leukocytes and endothelial cells, and both factors have been implicated in the promotion of hepatitis through induction of fibrin accumulation.²² In correspondence to the reduced clotting, we detected significantly diminished numbers of platelets in the livers of both mouse mutants. Previous studies have demonstrated a link between the intrahepatic activation of CD8⁺ T lymphocytes and platelet aggregation,³¹ which probably contributes to the hemostatic effects observed following ConA-mediated lymphocyte activation. Interestingly, RAG-2-deficient recipient mice of $\beta 7$ integrin-deficient lymphocytes developed less ConA-induced liver damage than RAG-2-deficient recipient mice of WT lymphocytes. Moreover, RAG-2/ $\beta 7$ integrin double-deficient recipient mice of WT lymphocytes developed less ConA-induced liver damage and intrasinusoidal clotting than similarly substituted RAG-2-deficient mice. These data point not only to the importance of lymphocytic $\beta 7$ integrin for the destructive process but also to a contribution of $\beta 7$ integrin-expressing innate immune cells such as macrophages or dendritic cells, which have been shown to promote ConA-induced autoimmune hepatitis.^{23,32} Of note, we and others have shown that $\beta 7$ integrin-expressing inflammatory monocytes exacerbate intestinal inflammation in mice and humans.^{33,34} In addition, activated KCs, on which we observed an upregulation of $\beta 7$ integrin, have

been reported to contribute to ConA-induced hepatitis through a Th1 type-dependent pathway.³⁵ Production of inflammatory cytokines, including tumor necrosis factor α , could well contribute to the inflammatory process by upregulating the expression of sinusoidal MAdCAM-1.

The fact that RAG-2-deficient mice receiving CD8⁺ T cells developed only very reduced liver damage, irrespective of the genotype of the cells transferred, suggests either that CD8⁺ T cells require an interaction with CD4⁺ T cells to exert a synergistic effect, or that $\beta 7$ integrin-expressing CD8⁺ T cells are of no importance in this experimental model.

One possible mechanism underlying the role of MAdCAM-1 in ConA-mediated hepatitis could therefore be that T cells adhering to the microvascular bed via MAdCAM-1/ $\beta 7$ integrin interactions may create an inflammatory environment within the sinusoids to which platelets can bind and aggregate and thus impair sinusoidal liver perfusion. In addition, MAdCAM-1-mediated endothelial interactions with lymphocytes such as $\alpha 4\beta 7$ integrin-expressing NKT cells or CD4⁺ T cells, cell types that have been shown to contribute to the pathology of ConA-induced hepatitis,^{36,37} will most likely cause an upregulation and accumulation of mediators that promote inflammation and exacerbate liver damage.

ConA-induced liver damage in WT mice was associated with increased hepatic MAdCAM-1 expression, a result that appears to contradict a report of Bonder et al,¹² in which the authors failed to detect MAdCAM-1 in murine liver after ConA administration. However, these authors used a lower concentration of ConA (13 mg/kg vs 20 mg/kg in our study) for induction of hepatitis and chose an earlier time for analysis (4 h after ConA injection vs 8 h in our study). Moreover, to detect MAdCAM-1, we used a tissue staining method with an increased sensitivity over standard detection methods (tyramide signal amplification [TSA] from PerkinElmer [Waltham, MA]). Because a striking strain difference has been demonstrated in ConA-induced hepatitis,³⁸ a subtle difference of genetic background may also influence results.

Figure 12. (See previous page). **Cellular adhesion of lymphocytes in liver sinusoids is reduced in ConA-treated MAdCAM-1-deficient mice.** Intravital 2-photon laser scanning microscopy following adoptive transfer of DsRed stained CD45⁺ cells and ConA injection. (A) Flow cytometric analysis of donor lymphocytes from DsRed mice. Lymphocyte preparations were controlled by staining a sample of these cells with an antibody cocktail containing anti-CD45, anti-CD19, and anti-CD3. The figure shows a representative FACS plot (left side) and the quantification of T cells (CD3⁺) and B cells (CD19⁺) (right side), accounting for 95% of the isolated CD45⁺ cells. (B–I) Cells were tracked over a time period of up to 2 hours and up to 3 independent view fields were recorded per animal. Fluorescent cells were detected by automated spot detection. Migration paths and speed of cells were tracked over time in (B) WT (CX3CR1^{+/eGFP}) and (C) MAdCAM-1 Δ/Δ (MAdCAM-1 Δ/Δ /CX3CR1^{+/eGFP}) mice. Fast movement is shown as pink tracks; slow movement is shown as turquoise tracks. Arrows indicate tracks. (D, E) Tracks derived from 2-photon laser scanning microscopy imaging shown in panels B and C were plotted using a common origin to depict overall motility of the cells. (F) Speed of individual spots and average track speed were analyzed statistically. Results shown are derived from 1 representative animal, calculating migration tracks from at least 3 independent view fields. Spots represent individual cells or tracks. (G) Cellular displacement from the point of origin and total track length were assessed to determine site-specific arrest of cells. (H) Statistical assessment of static cells with a track displacement of less than 5 μm . All experiments were performed in groups of 3 animals. Data represent mean \pm SD. Statistical significance was calculated by unpaired *t* test (**P* < .05; *****P* < .0001). (I) Representative screenshots from 2-photon laser scanning microscopy movies of CX3CR1^{+/eGFP} control and MAdCAM-1 Δ/Δ /CX3CR1^{+/eGFP} recipient mice, demonstrating that accumulation of DsRed-labeled cells is seen in periportal rather than pericentral areas, independent of the genotype. Scale bar = 50 μm . Donor lymphocytes are seen in red, CX3CR1-positive cells in green.

Another interesting finding is that ConA-mediated MAdCAM-1 induction only took place when $\beta 7$ integrin was expressed on lymphocytes and on innate immune cells, as shown by the lack of Madcam-1 upregulation in RAG-2-deficient mice after transfer of $\beta 7$ integrin-deficient lymphocytes and in RAG-2/ $\beta 7$ integrin double-deficient mice after transfer of $\beta 7$ integrin-deficient lymphocytes. The reduced MAdCAM-1 upregulation in these experimental settings correlated well with the comparably decreased liver damage. These results point to a contribution of $\beta 7$ integrin when expressed on innate and adaptive immune cells toward induction of MAdCAM-1 in the liver, thereby promoting the inflammatory process.

Interestingly, immunoneutralization of $\alpha 4$ integrin by mAb, although inhibiting the recruitment of inflammatory T cells to the liver, increased the severity of ConA-induced hepatitis, which the authors attribute to a decreased immigration of myeloid suppressor cells.³⁹ $\alpha 4$ integrin forms heterodimers with either the $\beta 1$ ($\alpha 4\beta 1$) or the $\beta 7$ ($\alpha 4\beta 7$) integrin subunit, binding preferentially to VCAM-1 or MAdCAM-1, respectively. Since MAdCAM-1 as well as $\beta 7$ integrin deficiency ameliorates ConA-induced hepatitis, it is tempting to speculate that $\alpha 4\beta 7$ integrin deficiency provides protection from hepatitis by disturbing lymphocyte interactions with endothelial MAdCAM-1, while protection through recruitment of $\alpha 4\beta 1$ -VCAM-1 myeloid suppressor cells is still feasible. However, treatment with anti-VCAM-1 monoclonal antibody did not cause an exacerbation of ConA-induced hepatitis, and in one report was even shown to attenuate ConA-induced hepatitis,¹⁰ while producing no effect in another.⁴⁰ These results hint at the involvement of additional disease promoting, VCAM-1-mediated processes, mediated by different VCAM-1 binding partners such as $\alpha 4\beta 7$ integrin.

The fact that MAdCAM-1 deficiency ameliorates ConA-mediated hepatitis to an even greater extent than $\beta 7$ integrin deficiency could mean that not only interactions of MAdCAM-1 and $\beta 7$ integrin, but also interactions of MAdCAM-1 with additional receptors such as L-selectin may contribute to the inflammatory process. An involvement of L-selectin in ConA-mediated hepatitis, most probably mediated via CD4⁺ T cells, has already been established.⁶ In addition, neutrophils, which exhibit a constitutively high expression of L-selectin, have been shown to promote the ConA-mediated pathology.⁴¹ This promiscuity of receptor and ligand interactions adds complexity to our understanding of the physiologic roles of the respective adhesion molecules.

In conclusion, we have demonstrated that beyond their roles in promoting IBD and experimental NASH,²⁰ $\alpha 4\beta 7$ /MAdCAM-1 interactions also contribute to the pathogenesis of acute immune-driven hepatitis by facilitating lymphocyte and sinusoidal endothelial cell interaction and thereby promoting sinusoidal clotting and liver injury. Our study thus contributes to a better understanding of immune cell adhesion pathways associated with the pathogenesis of liver inflammation and points to MAdCAM-1 and $\alpha 4\beta 7$ integrin as potential targets for specific antiadhesive drugs in immune-mediated hepatitis.

Materials and Methods

Ethical Statement

All experiments were approved by the local Institutional Animal Care and Research Advisory Committee and authorized by the regional government authorities for nature and environmental and consumer protection of North Rhine-Westphalia (LANUV [Landesamt für Natur, Umwelt und Verbraucherschutz] North Rhine-Westphalia), Recklinghausen, Germany (approval # 84-02.04.2013.A054). All experiments were performed in accordance with the German guidelines for animal housing and husbandry.

Mice

All experiments were performed with male, age-matched mice of C57BL/6 J background and similar weight using 10- to 12-week-old MAdCAM-1-deficient (MAdCAM-1 Δ/Δ) mice (B6.129-Madcam1^{tm1.2Nwag}),⁴² $\beta 7$ integrin-deficient ($\beta 7$ Δ/Δ) mice (C57BL/6-Itgb^{tm1Cgn}/J),¹⁴ RAG-2-deficient (RAG-2 Δ/Δ) mice (RAG-2tm/J),⁴³ RAG-2 Δ/Δ - $\beta 7$ Δ/Δ double-deficient mice, RAG-2 Δ/Δ -MAdCAM-1 Δ/Δ mice, DsRed (B6.Cg-Tg(CAG-DsRed**MST*)1Nagy/J) mice,²⁷ CX3CR1^{+/GFP} (B6.129P-Cx3cr1^{tm1Litt}/J)²⁶ mice, MAdCAM-1 Δ/Δ /CX3CR1^{+/GFP} mice, and age-matched C57BL/6 J (WT) mice. The CX3CR1^{+/GFP} mice had GFP (green fluorescent protein) inserted into the CX3CR1 locus.²⁶ The animals were bred at RWTH Aachen University under specific pathogen-free conditions.

ConA Administration

ConA (Sigma-Aldrich, Taufkirchen, Germany) was dissolved in sterile, pyrogen-free phosphate-buffered saline (PBS) and intravenously injected once via the tail vein at a concentration of 20 mg/kg body weight.

Intravital 2-Photon Microscopy

Liver intravital 2-photon laser scanning microscopy was performed as described previously.^{44,45} In brief, animals were initially anesthetized by intraperitoneal injection of ketamine/xylazine (100 and 10 mg/kg), followed by tracheotomy and controlled respiration (2.5% isoflurane in 100% O₂). The liver was exposed laparotomically and was monitored by video microscopy for a time period of up to 2 hours, imaging multiple view fields. Capillary blood flow was monitored by light microscopy at regular intervals of 30 minutes to rule out artefacts caused by breakdown of sinusoidal perfusion. Cellular motility was assessed by determining speed and displacement of Actin-DsRed⁺ lymphocytes. For tracking, 3 × 10⁷ cells were adoptively transferred after the setting up of single-cell suspensions prepared from lymph nodes of Actin-DsRed mice.²⁷ Cells were then followed over the time course of the imaging. The time stamp within the images shows the time lapse for each sequence, the increment was usually around 30 seconds per full scan (xyz) and differed only slightly between experiments, and tracking was normalized to the actual time between images for calculation of speed parameters. Video sequence analysis and reconstruction were performed using

Table 1. Antibodies Used for FACS Analysis

Antibody	Clone	Manufacturer
CD3	145-2C11	eBioscience, San Diego, CA
CD4	GK1.5	BD Biosciences, Heidelberg, Germany
CD8	53-6.7	eBioscience, San Diego, CA; BioLegend, San Diego CA; BD Biosciences, Heidelberg, Germany
CD11b	M1/70	BD Biosciences, Heidelberg, Germany; eBioscience, San Diego, CA
CD11c	N418	eBioscience, San Diego, CA
CD19	1D3	eBioscience, San Diego, CA
CD41	MWRReg30	BD Biosciences, Heidelberg, Germany
CD45	GK1.5	BD Biosciences, Heidelberg, Germany
CD69	H1.2F3	eBioscience, San Diego, CA
CD142 (TF)	LS-C417788	LSBio, Seattle, WA
CD146 APC	ME-9F1	Miltenyi Biotec, Bergisch Gladbach, Germany
CD161 (NK1.1)	PK136	eBioscience, San Diego, CA
CD206	C0658C2	BioLegend, San Diego, USA
CD317 (PDCA-1)	eBio927	eBioscience, San Diego, CA
β 7	M293	BD Biosciences, Heidelberg
β catenin		
Gr-1	RB6-8C5	BD Biosciences, Heidelberg, Germany
Ly6G	1A8	BD Biosciences, Heidelberg, Germany
F4/80	BM8	eBioscience, San Diego, CA
PAI-1	ab66705	Abcam, Cambridge, United Kingdom
Streptavidin APC	554076	BD Biosciences, Heidelberg, Germany
Anti-rat Cy3	Polyclonal	Jackson ImmunoResearch, Cambridge, United Kingdom
Anti-mouse FITC	Polyclonal	Jackson ImmunoResearch, Cambridge, United Kingdom

PAI, plasminogen activator inhibitor-1; TF, tissue factor.

IMARIS (7.7 and 8.3; Bitplane AG, Zürich, Switzerland) and Fiji software (version 1.48s; ImageJ, US National Institutes of Health, Bethesda, MD).

Histological Evaluation, Apoptosis Determination, and Immunofluorescence Staining

Following fixation with 10% formalin/PBS, livers were embedded in paraffin; 4- μ m paraffin sections were serially cut, mounted onto glass slides, deparaffinized, and stained with H&E. Blinded histological scoring for hepatic necrosis was assessed in each section as the percentage of liver parenchyma with necrotic change. Nine to 12 microscopic fields (magnification 10 \times) were taken from each section. The total hepatic parenchymal area and the necrotic area were estimated by means of a size marker using ImageJ software (version 1.50; National Institutes of Health, Bethesda, MD),⁴⁶ and the extent of necrosis as a percentage of the total area was calculated for each experimental group. Clotting was quantified by color deconvolution of H&E-stained samples followed by threshold setting. The total area of each sample was then determined by encircling the section area, and the percentage of clotting of the total area was measured by ImageJ software (version 1.52p).⁴⁶

Apoptosis was evaluated on frozen sections by TUNEL assay using an in situ cell death detection kit (Fluorescein;

Roche Diagnostic, Mannheim, Germany) according to the manufacturer's instructions. Ten images (magnification 10 \times) were randomly obtained from each liver section. TUNEL-positive cells were counted (using ImageJ, version 1.50),⁴⁶ and the average number of TUNEL-positive cells for each section together with the mean value for each experimental group was established.

For immunofluorescence staining for MAdCAM-1, acetone-fixed cryostat sections of the liver were quenched with 0.3% H₂O₂ in PBS and blocked with 2% goat serum and 5% bovine serum albumin (BSA) in TBST⁺⁺ (0.1 M Tris, pH 7.5, 0.15 M NaCl, 0.05% Tween 20, 1 mM MgCl₂, 0.1 mM CaCl₂). Sections were then incubated overnight with purified rat anti-mouse MAdCAM-1 (BD Biosciences, Heidelberg, Germany) diluted in 2% BSA in TBST⁺⁺. Subsequently, sections were incubated with anti-rat IgG horseradish peroxidase-linked antibody (GE Healthcare, Buckinghamshire, UK). For TSA, sections were incubated in TSA Plus working solution (TSA Plus Fluorescein Kit; PerkinElmer). In case of double stainings, sections were incubated with anti-CD146 (Miltenyi Biotec, Bergisch Gladbach, Germany). Immunofluorescence staining of acetone-fixed cryostat sections of the liver without using TSA, sections were quenched with 50-mM NH₄Cl in TBST⁺⁺ and blocked with 5% BSA in TBST⁺⁺. Sections were incubated with the following antibodies: purified rabbit anti-mouse PAI-1 (Abcam,

Table 2. Oligonucleotides for Real-Time PCR Analysis

Gene		Sequence
<i>β-actin</i>	Sense 5' → 3'	ACT ATT GGC AAC GAG CGG TTC
	Antisense 3' → 5'	TTA CGG ATG TCA ACG TCA CAC TTC
<i>lfn-γ</i>	Sense 5' → 3'	GAG GTC AAC AAC CCA CAG GTC
	Antisense 3' → 5'	CGA ATC AGC AGC GAC TCC T
<i>Il-2</i>	Sense 5' → 3'	GAC CTG TGC GGC ATG TTC TG
	Antisense 3' → 5'	TCA TCG AAT TGG CAC TCA AAT G
<i>IL-6</i>	Sense 5' → 3'	TGA GAT CTA CTC GGC AAA CCT AGT G
	Antisense 3' → 5'	CTT CGT AGA GAA CAA CAT AAG TCA GAT ACC
<i>Mcp-1</i>	Sense 5' → 3'	AGA GCC AGA CGG GAG GAA G
	Antisense 3' → 5'	CCA GCC TAC TCA TTG GGA TC
<i>Mip-1-α</i>	Sense 5' → 3'	TAC AAG CAG CAG CGA GTA CC
	Antisense 3' → 5'	TCA GGA AAA TGA CAC CTG GCT
<i>Perforin</i>	Sense 5' → 3'	GAT GTG AAC CCT AGG CCA GA
	Antisense 3' → 5'	GGT TTT TGT ACC AGG CGA AA
<i>Granzyme B</i>	Sense 5' → 3'	ATC CTG CTC TGA TTA CCC ATC GT
	Antisense 3' → 5'	ATG GAT ATG AAG CCA GTC TTT GC
<i>Eotaxin</i>	Sense 5' → 3'	ATT GTG TTG TTT GTT TGC TTG C
	Antisense 3' → 5'	GTC AGC CTG GTC TAC ACA GTG A
<i>Tgf-β</i>	Sense 5' → 3'	GGA CCC TGC CCC TAT ATT TGG
	Antisense 3' → 5'	TGT TGC AGG TCA TTT AAC CAA GTG
<i>Tnf-α</i>	Sense 5' → 3'	AGA AAC ACA AGA TGC TGG GAC AGT
	Antisense 3' → 5'	CCT TTG CAG AAC TCA GGA ATG G
<i>Madcam-1</i>	Sense 5' → 3'	GCA TGG TGA CCT GGC AGT GAA
	Antisense 3' → 5'	CAT GTC TCT CCT ATG ACG ACG G
<i>iNos</i>	Sense 5' → 3'	GGG CAG CCT GTG AGA CCT T
	Antisense 3' → 5'	TGA AGC GTT TCG GGA TCT G
<i>Il-4</i>	Sense 5' → 3'	AG GTC ACA GGA GAA GGG ACG CC
	Antisense 3' → 5'	CCC GAA GGT TCC ACG AAG CGT
<i>Tf</i>	Sense 5' → 3'	TGT GCA CCG AGC AAT GGA A
	Antisense 3' → 5'	AGG TAT AGA GAC ACG TTC G
<i>Pai-1</i>	Sense 5' → 3'	TGC TGA ACT CAT CAG ACA ATG GAA G
	Antisense 3' → 5'	AAT CAC GTT GGG ACC GGC T
<i>Fizz</i>	Sense 5' → 3'	GGTCCCAGTGCATATGGATGAGACCATAGA
	Antisense 3' → 5'	CACCTTCTCACTCGAGGGACAGTTGGCAGC
<i>Cd38</i>	Sense 5' → 3'	CACCAGGATCCCTCATGACT
	Antisense 3' → 5'	TCCTTCTGTCCGGATTACTG
<i>Pparg</i>	Sense 5' → 3'	TGT CGG TTT CAG AAG TGC CTT G
	Antisense 3' → 5'	TTC AGC TGG TCG ATA TCA CTG GAG
<i>Arg</i>	Sense 5' → 3'	CAGAAGAATGGAAGAGTCAG
	Antisense 3' → 5'	CAGATATGCAGGGAGTCACC

FACS, fluorescence-activated cell sorting; IL, interleukin; PCR, polymerase chain reaction.

Cambridge, United Kingdom), biotinylated anti-Tissue Factor (LSBio, Seattle, WA) or purified rat anti-mouse CD41 (BD Biosciences), and purified mouse anti-β-Catenin (BD Biosciences, Heidelberg, Germany) or APC coupled anti-mouse CD146 (Miltenyi Biotec, Bergisch Gladbach, Germany) in 2% BSA in TBST⁺⁺. Subsequently, the sections were incubated with the respective secondary antibody: AF488 goat anti-rabbit (Santa Cruz Biotechnology, Dallas, TX), APC Streptavidin (BD Biosciences), Cy3 mouse anti-rat, or FITC

anti-mouse (both from Jackson ImmunoResearch, Cambridge, United Kingdom) in 2% BSA in TBST⁺⁺. Tissue samples were finally counterstained with DAPI and mounted with Fluoromount-G (SouthernBiotech, Birmingham, AL).

Images were acquired using an Axioplan2 fluorescence microscope (Carl Zeiss Microscopy, Oberkochen, Germany) and VisiView software (2.0.3) (Visitron Systems, Puchheim, Germany). Area covered by the respective stain was quantified automatically using FIJI ImageJ software version 1.50.⁴⁶

Flow Cytometry

Cell isolation and surface staining were performed as described previously.^{14,47} Mononuclear liver cells were stained directly using combinations of the following monoclonal antibodies: anti-CD3, anti-CD8a, anti-CD19, anti-CD11b, anti-CD11c, anti-CD69, anti-CD161, anti-CD317, anti-F4/80, anti-Ly6G, anti-CD4, anti-CD8, anti-CD11b, anti-CD45, and anti-CD206, listed in Table 1. Cells were measured on a FACS (fluorescence-activated cell sorting) Canto-II cytometer (BD Biosciences). Data were analyzed by FlowJo 8.7.3 and 10.2 software (Tree Star, Ashland, OR).

Lymphocyte Isolation and Adoptive Cell Transfer

Cells for lymphocyte transfer were obtained from peripheral and mesenteric lymph nodes. Single cell suspensions were obtained by mechanically mincing through a 100- μ m cell strainer. A total of 7.65×10^6 lymphocytes from $\beta 7$ integrin-deficient ($\beta 7 \Delta/\Delta$) mice (C57BL/6-Itgb^{tm1Cgn/J})¹⁴ or WT mice (C57BL/6J) mice were intravenously transferred to RAG-2-deficient (RAG-2 Δ/Δ) mice (RAG-2^{tm/J}), RAG-2 Δ/Δ - $\beta 7 \Delta/\Delta$ double-deficient mice or RAG-2 Δ/Δ -MAdCAM-1 Δ/Δ mice.

Cells for CD4⁺ and CD8⁺ T transfer were isolated from spleen, mesenteric lymph nodes, and peripheral lymph nodes by magnetic cell separation (MACS; Miltenyi Biotec) according to the manufacturers' instructions. Briefly, single-cell suspensions from lymph nodes and spleen were pooled, after erythrocyte lysis with lysis buffer (BD Pharmingen, San Jose, CA). CD4⁺ and CD8⁺ T cells were purified by MACS using biotinylated antibodies, followed by anti-biotin microbeads and separation via MACS columns according to the manufacturer's instructions. Purity of the isolated cell fractions was controlled by flow cytometry and was consistently >92%. The cells were resuspended in an appropriate volume of sterile PBS and mixed allowing for 0.895×10^6 CD8⁺ and 1.450×10^6 CD4⁺ T cells or 1.79×10^6 CD8⁺ T cells per tail vein injection per mouse. T cell numbers for mixed transfer were based on back calculation of the T cell ratio in the whole lymphocyte population. For CD8⁺ T cell transfer, the number was doubled.

Quantification of Cytokines and Chemokines

Total RNA isolations from the liver and complementary DNA synthesis were performed as described previously.⁴⁸ RT-PCR was performed in duplicate in a total volume of 20 μ L on a 7300 RT-PCR system with 7000 System SDS Software Version 1.2.3 (Applied Biosystems, Darmstadt, Germany) using the quantitative PCR Master Mix for SYBR Green I (Eurogentec, Cologne, Germany). Primer sequences are listed in Table 2. β -actin was used as endogenous control for normalization. Expression levels of the target genes are displayed as values relative to the levels found in control animals (ie, untreated C57BL/6, $\beta 7 \Delta/\Delta$, or MAdCAM-1 Δ/Δ mice).

Data Analysis

Statistical analyses were performed with GraphPad Prism software (version 5; GraphPad Software, San Diego,

CA). Data are presented as mean \pm SEM, unless otherwise indicated. The specific statistical tests are indicated in the respective figure legends.

Access to Data

All authors had access to the study data and had reviewed and approved the final manuscript.

References

1. Tiegs G, Hentschel J, Wendel A. A T cell-dependent experimental liver injury in mice inducible by concanavalin A. *J Clin Invest* 1992;90:196–203.
2. Küsters S, Gantner F, Künstle G, Tiegs G. Interferon gamma plays a critical role in T cell-dependent liver injury in mice initiated by concanavalin A. *Gastroenterology* 1996;111:462–471.
3. Mizuhara H, O'Neill E, Seki N, Ogawa T, Kusunoki C, Otsuka K, Satoh S, Niwa M, Senoh H, Fujiwara H. T cell activation-associated hepatic injury: mediation by tumor necrosis factors and protection by interleukin 6. *J Exp Med* 1994;179:1529–1537.
4. Toyabe S, Seki S, Iiai T, Takeda K, Shirai K, Watanabe H, Hiraide H, Uchiyama M, Abo T. Requirement of IL-4 and liver NK1+ T cells for concanavalin A-induced hepatic injury in mice. *J Immunol* 1997;159:1537–1542.
5. Springer TA. Traffic signals for lymphocyte recirculation and leukocyte emigration: the multistep paradigm. *Cell* 1994;76:301–314.
6. Kawasuji A, Hasegawa M, Horikawa M, Fujita T, Matsushita Y, Matsushita T, Fujimoto M, Steeber DA, Tedder TF, Takehara K, Sato S. L-selectin and intercellular adhesion molecule-1 regulate the development of Concanavalin A-induced liver injury. *J Leukoc Biol* 2006;79:696–705.
7. Massaguer A, Perez-Del-Pulgar S, Engel P, Serratos J, Bosch J, Pizcueta P. Concanavalin-A-induced liver injury is severely impaired in mice deficient in P-selectin. *J Leukoc Biol* 2002;72:262–270.
8. Volpes R, Van Den Oord JJ, Desmet VJ. Vascular adhesion molecules in acute and chronic liver inflammation. *Hepatology* 1992;15:269–275.
9. Adams DH, Hubscher SG, Fisher NC, Williams A, Robinson M. Expression of E-selectin and E-selectin ligands in human liver inflammation. *Hepatology* 1996;24:533–538.
10. Morikawa H, Hachiya K, Mizuhara H, Fujiwara H, Nishiguchi S, Shiomi S, Kuroki T, Kaneda K. Sublobular veins as the main site of lymphocyte adhesion/transmigration and adhesion molecule expression in the porto-sinusoidal-hepatic venous system during concanavalin A-induced hepatitis in mice. *Hepatology* 2000;31:83–94.
11. Matsumoto G, Tsunematsu S, Tsukinoki K, Ohmi Y, Iwamiya M, Oliveira-dos-Santos A, Tone D, Shindo J, Penninger JM. Essential role of the adhesion receptor LFA-1 for T cell-dependent fulminant hepatitis. *J Immunol* 2002;169:7087–7096.
12. Bonder CS, Norman MU, Swain MG, Zbytnik LD, Yamanouchi J, Santamaria P, Ajuebor M, Salmi M,

- Jalkanen S, Kubes P. Rules of recruitment for Th1 and Th2 lymphocytes in inflamed liver: a role for alpha-4 integrin and vascular adhesion protein-1. *Immunity* 2005;23:153–163.
13. Gorfu G, Rivera-Nieves J, Ley K. Role of beta7 integrins in intestinal lymphocyte homing and retention. *Curr Mol Med* 2009;9:836–850.
 14. Wagner N, Löhler J, Kunkel EJ, Ley K, Leung E, Krissansen G, Rajewsky K, Müller W. Critical role for beta7 integrins in formation of the gut-associated lymphoid tissue. *Nature* 1996;382:366–370.
 15. Karlsen TH, Folseraas T, Thorburn D, Vesterhus M. Primary sclerosing cholangitis - a comprehensive review. *J Hepatol* 2017;67:1298–1323.
 16. Ala A, Brown D, Khan K, Standish R, Odin JA, Fiel MI, Schiano TD, Hillan KJ, Rahman SA, Hodgson HJ, Dhillon AP. Mucosal addressin cell adhesion molecule (MAdCAM-1) expression is up-regulated in the cirrhotic liver and immunolocalises to the peribiliary plexus and lymphoid aggregates. *Dig Dis Sci* 2013;58:2528–2541.
 17. Hillan KJ, Hagler KE, MacSween RN, Ryan AM, Renz ME, Chiu HH, Ferrier RK, Bird GL, Dhillon AP, Ferrell LD, Fong S. Expression of the mucosal vascular addressin, MAdCAM-1, in inflammatory liver disease. *Liver* 1999;19:509–518.
 18. Grant AJ, Lalor PF, Hubscher SG, Briskin M, Adams DH. MAdCAM-1 expressed in chronic inflammatory liver disease supports mucosal lymphocyte adhesion to hepatic endothelium (MAdCAM-1 in chronic inflammatory liver disease). *Hepatology* 2001;33:1065–1072.
 19. Eksteen B, Miles AE, Grant AJ, Adams DH. Lymphocyte homing in the pathogenesis of extra-intestinal manifestations of inflammatory bowel disease. *Clin Med (Lond)* 2004;4:173–180.
 20. Drescher HK, Schippers A, Clahsen T, Sahin H, Noels H, Hornef M, Wagner N, Trautwein C, Streetz KL, Kroy DC. beta7-Integrin and MAdCAM-1 play opposing roles during the development of non-alcoholic steatohepatitis. *J Hepatol* 2017;66:1251–1264.
 21. Miyazawa Y, Tsutsui H, Mizuhara H, Fujiwara H, Kaneda K. Involvement of intrasinusoidal hemostasis in the development of concanavalin A-induced hepatic injury in mice. *Hepatology* 1998;27:497–506.
 22. Kato J, Okamoto T, Motoyama H, Uchiyama R, Kirchhofer D, Van Rooijen N, Enomoto H, Nishiguchi S, Kawada N, Fujimoto J, Tsutsui H. Interferon-gamma-mediated tissue factor expression contributes to T-cell-mediated hepatitis through induction of hypercoagulation in mice. *Hepatology* 2013;57:362–372.
 23. Nakamoto N, Ebinuma H, Kanai T, Chu PS, Ono Y, Mikami Y, Ojio K, Lipp M, Love PE, Saito H, Hibi T. CCR9+ macrophages are required for acute liver inflammation in mouse models of hepatitis. *Gastroenterology* 2012;142:366–376.
 24. Heymann F, Hamesch K, Weiskirchen R, Tacke F. The concanavalin A model of acute hepatitis in mice. *Lab Anim* 2015;49:12–20.
 25. Yu Z, Otsuka H, Yamaguchi K, Kuroishi T, Sasano T, Sugawara S, Nakamura M, Endo Y. Roles of platelets and macrophages in the protective effects of lipopolysaccharide against concanavalin A-induced murine hepatitis. *Biochim Biophys Acta* 2011;1812:1069–1079.
 26. Jung S, Aliberti J, Graemmel P, Sunshine MJ, Kreutzberg GW, Sher A, Littman DR. Analysis of fractalkine receptor CX(3)CR1 function by targeted deletion and green fluorescent protein reporter gene insertion. *Mol Cell Biol* 2000;20:4106–4114.
 27. Vintersten K, Monetti C, Gertsenstein M, Zhang P, Laszlo L, Biechele S, Nagy A. Mouse in red: red fluorescent protein expression in mouse ES cells, embryos, and adult animals. *Genesis* 2004;40:241–246.
 28. Lycke J. Monoclonal antibody therapies for the treatment of relapsing-remitting multiple sclerosis: differentiating mechanisms and clinical outcomes. *Ther Adv Neurol Disord* 2015;8:274–293.
 29. Danese S, Panes J. Development of drugs to target interactions between leukocytes and endothelial cells and treatment algorithms for inflammatory bowel diseases. *Gastroenterology* 2014;147:981–989.
 30. Liaskou E, Karikoski M, Reynolds GM, Lalor PF, Weston CJ, Pullen N, Salmi M, Jalkanen S, Adams DH. Regulation of mucosal addressin cell adhesion molecule 1 expression in human and mice by vascular adhesion protein 1 amine oxidase activity. *Hepatology* 2011;53:661–672.
 31. Guidotti LG, Inverso D, Sironi L, Di Lucia P, Fioravanti J, Ganzer L, Fiocchi A, Vacca M, Aiolfi R, Sammicheli S, Mainetti M, Cataudella T, Raimondi A, Gonzalez-Aseguinolaza G, Protzer U, Ruggeri ZM, Chisari FV, Isogawa M, Sitia G, Iannacone M. Immunosurveillance of the liver by intravascular effector CD8(+) T cells. *Cell* 2015;161:486–500.
 32. Wang J, Cao X, Zhao J, Zhao H, Wei J, Li Q, Qi X, Yang Z, Wang L, Zhang H, Bai L, Wu Z, Zhao L, Hong Z, Yin Z. Critical roles of conventional dendritic cells in promoting T cell-dependent hepatitis through regulating natural killer T cells. *Clin Exp Immunol* 2017;188:127–137.
 33. Schippers A, Muschaweck M, Clahsen T, Tautorat S, Grieb L, Tenbrock K, Gassler N, Wagner N. beta7-Integrin exacerbates experimental DSS-induced colitis in mice by directing inflammatory monocytes into the colon. *Mucosal Immunol* 2016;9:527–538.
 34. Zeissig S, Rosati E, Dowds CM, Aden K, Bethge J, Schulte B, Pan WH, Mishra N, Zuhayra M, Marx M, Paulsen M, Strigli A, Conrad C, Schuldt D, Sinha A, Ebsen H, Kornell SC, Nikolaus S, Arlt A, Kabelitz D, Ellrichmann M, Lutzen U, Rosenstiel PC, Franke A, Schreiber S. Vedolizumab is associated with changes in innate rather than adaptive immunity in patients with inflammatory bowel disease. *Gut* 2019;68:25–39.
 35. Chen L, Xie XJ, Ye YF, Zhou L, Xie HY, Xie QF, Tian J, Zheng SS. Kupffer cells contribute to concanavalin A-induced hepatic injury through a Th1 but not Th17 type response-dependent pathway in mice. *Hepatobiliary Pancreat Dis Int* 2011;10:171–178.
 36. Takeda K, Hayakawa Y, Van Kaer L, Matsuda H, Yagita H, Okumura K. Critical contribution of liver natural

- killer T cells to a murine model of hepatitis. *Proc Natl Acad Sci U S A* 2000;97:5498–5503.
37. Xiang M, Liu T, Tan W, Ren H, Li H, Liu J, Cao H, Cheng Q, Liu X, Zhu H, Tuo Y, Wang J, Zhang Y. Effects of kinse-noside, a potential immunosuppressive drug for autoimmune hepatitis, on dendritic cells/CD8⁺ T cells communication in mice. *Hepatology* 2016;64:2135–2150.
 38. Mizuhara H, Kuno M, Seki N, Yu WG, Yamaoka M, Yamashita M, Ogawa T, Kaneda K, Fujii T, Senoh H, Fujiwara H. Strain difference in the induction of T-cell activation-associated, interferon gamma-dependent hepatic injury in mice. *Hepatology* 1998;27:513–519.
 39. Lee WY, Salmi M, Kelly MM, Jalkanen S, Kubes P. Therapeutic advantage of anti-VAP-1 over anti-alpha4 integrin antibody in concanavalin A-induced hepatitis. *Hepatology* 2013;58:1413–1423.
 40. Wolf D, Hallmann R, Sass G, Sixt M, Küsters S, Fregien B, Trautwein C, Tiegs G. TNF-alpha-induced expression of adhesion molecules in the liver is under the control of TNFR1—relevance for concanavalin A-induced hepatitis. *J Immunol* 2001;166:1300–1307.
 41. Bonder CS, Ajuebor MN, Zbytniuk LD, Kubes P, Swain MG. Essential role for neutrophil recruitment to the liver in concanavalin A-induced hepatitis. *J Immunol* 2004;172:45–53.
 42. Schippers A, Leuker C, Pabst O, Kochut A, Prochnow B, Gruber AD, Leung E, Krissansen GW, Wagner N, Müller W. Mucosal addressin cell-adhesion molecule-1 controls plasma-cell migration and function in the small intestine of mice. *Gastroenterology* 2009;137:924–933.
 43. Shinkai Y, Rathbun G, Lam KP, Oltz EM, Stewart V, Mendelsohn M, Charron J, Datta M, Young F, Stall AM, Alt FW. RAG-2-deficient mice lack mature lymphocytes owing to inability to initiate V(D)J rearrangement. *Cell* 1992;68:855–867.
 44. Mossanen JC, Krenkel O, Ergen C, Govaere O, Liepelt A, Püngel T, Heymann F, Kalthoff S, Lefebvre E, Eulberg D, Lüdde T, Marx G, Strassburg CP, Roskams T, Trautwein C, Tacke F. Chemokine (C-C motif) receptor 2-positive monocytes aggravate the early phase of acetaminophen-induced acute liver injury. *Hepatology* 2016;64:1667–1682.
 45. Heymann F, Niemietz PM, Peusquens J, Ergen C, Kohlhepp M, Mossanen JC, Schneider C, Vogt M, Tolba RH, Trautwein C, Martin C, Tacke F. Long term intravital multiphoton microscopy imaging of immune cells in healthy and diseased liver using CXCR6.Gfp reporter mice. *J Vis Exp* 2015;97:52607.
 46. Schneider CA, Rasband WS, Eliceiri KW. NIH Image to ImageJ: 25 years of image analysis. *Nat Methods* 2012; 9:671–675.
 47. Karlmark KR, Weiskirchen R, Zimmermann HW, Gassler N, Ginhoux F, Weber C, Merad M, Luedde T, Trautwein C, Tacke F. Hepatic recruitment of the inflammatory Gr1⁺ monocyte subset upon liver injury promotes hepatic fibrosis. *Hepatology* 2009; 50:261–274.
 48. Pils MC, Bleich A, Prinz I, Fasnacht N, Bollati-Fogolin M, Schippers A, Rozell B, Müller W. Commensal gut flora reduces susceptibility to experimentally induced colitis via T-cell-derived interleukin-10. *Inflamm Bowel Dis* 2011;17:2038–2046.

Received May 4, 2020. Accepted December 4, 2020.

Correspondence

Address Correspondence to: Norbert Wagner, MD, Department of Pediatrics, RWTH Aachen University, Pauwelsstrasse 30, D-52074 Aachen, Germany. e-mail: nwagner@ukaachen.de; fax: +49 241-8082492.

Acknowledgments

The authors thank Kerstin Eßer for expert technical help. The authors thank the Core Facility Two-Photon Microscopy and the Core Facility Immunohistochemistry, Core Facilities of the Interdisciplinary Center for Clinical Research Aachen within the Faculty of Medicine at RWTH Aachen University for their support.

CRedit Authorship Contributions

Angela Schippers (Conceptualization: Equal; Funding acquisition: Equal; Investigation: Lead; Writing – original draft: Lead; Writing – review & editing: Equal)

Jessica Hübel (Data curation: Equal; Investigation: Equal; Methodology: Equal; Software: Equal)

Felix Heymann (Data curation: Equal; Investigation: Equal; Methodology: Equal; Software: Equal)

Thomas Clahsen (Data curation: Equal; Investigation: Supporting; Methodology: Equal)

Sreepradha Eswaran (Data curation: Equal; Methodology: Equal)

Sarah Schlepütz (Investigation: Supporting; Methodology: Supporting)

Robin Püllen (Investigation: Supporting; Methodology: Supporting)

Nikolaus Gaßler (Formal analysis: Supporting; Methodology: Supporting)

Klaus Tenbrock (Writing – review & editing: Supporting)

Frank Tacke (Formal analysis: Supporting; Writing – review & editing: Supporting)

Norbert Wagner, M.D. (Conceptualization: Equal; Funding acquisition: Equal; Writing – original draft: Supporting; Writing – review & editing: Equal)

Conflicts of Interest

The authors disclose no conflicts.

Funding

This research was supported by the START-Program of the Faculty of Medicine (141/15), RWTH Aachen; German Research Foundation grants SCHI 1170/2-1, TA 434/5-1, and WA.1127/4-1; the Interdisciplinary Center for Clinical Research Consortium Organ Crosstalk E8-8, and the German Research Foundation Project-ID 403324012 – SFB 1382.

Supplementary Material

Supplementary Videos 1 and 2. MAdCAM-1 deficiency reduces cellular adhesion of lymphocytes in liver sinusoids following concanavalin A (ConA)-induced liver damage. Intravital 2-photon laser scanning microscopy was performed on mouse livers following adoptive transfer of 3×10^7 CD45⁺ cells isolated from lymph nodes of Actin-DsRed donor mice. Cells were intravenously injected directly before the surgery performed for 2-photon laser scanning microscopy imaging. A total of 20/mg/kg ConA was applied by intracardiac injection in a total volume of 100 μ L, and 2-photon laser scanning

microscopy imaging was commenced directly afterward. Owing to the transgenic green fluorescent protein expression, circulating monocytes and liver resident dendritic cells are visible in green, Actin-DsRed donor mice-derived T cells are in red, and collagen structures appear blue. Fast movement is shown as pink tracks; slow movement is shown as turquoise tracks. Cells were tracked over a time period of up to 2 hours. Movies show recordings of 1 representative view field of liver from a (M1) wild-type (CX3CR1^{+eGFP}) mouse and a (M2) MAdCAM-1 Δ/Δ (MAdCAM-1 Δ/Δ / CX3CR1^{+eGFP}) mouse. Fluorescent cells were detected by automated spot detection using Imaris 8.3.